Part III

Beyond cognitive radar—from theory to practice

Chapter 13

One-bit cognitive radar

Arindam Bose[1], Jian Li[2] and Mojtaba Soltanalian[1]

Target parameter estimation in active sensing, and particularly radar signal processing, is a long-standing problem that has been studied extensively. In this chapter, a novel approach for target parameter estimation is discussed for cases where one-bit analog-to-digital-converters (ADCs), also known as signal comparators with time-varying thresholds, are employed to sample the received radar signal instead of high-resolution ADCs. The considered problem has potential applications in the design of inexpensive radar and sensing devices in civilian applications and paves the way for future radar systems employing low-resolution ADCs for faster sampling and high-resolution target determination. The target estimation has been formulated as a multivariate weighted least-squares optimization problem that can be solved in a cyclic manner.

Additionally, an important problem in cognitive radar is to enhance the estimation performance of the system by a joint design of its probing signal and receive filter using the a priori information on interference. In such cases, the knowledge of interference statistics (particularly the covariance) plays a vital role in an effective design of the radar waveforms. In most practical scenarios, however, the received signal and interference statistics are available subject to some uncertainty. Particularly, an extreme manifestation of this practical observation occurs for radars employing one-bit receivers, where only a normalized version of the interference covariance matrix can be obtained. This chapter also formulates a waveform optimization problem and discusses an algorithm to design the transmit waveform and the receive filter of one-bit radars given such uncertainties in acquired interference statistics. The effectiveness of the proposed algorithms is corroborated through numerical analysis.

13.1 Introduction

The problem of target parameter estimation permeates the field of active sensing and radar signal processing. Active sensing systems aim to uncover the location and other useful properties such as velocity information and reflectance properties of a target of interest by dispatching a transmit waveform toward the target and studying

[1]University of Illinois at Chicago, USA
[2]University of Florida, USA

AQ1

the received echo reflected by it. For example, the complete dynamics of a moving vehicle including its location and velocity with respect to the observer can easily be found by simply measuring the difference between the transmitted and received electromagnetic waves in the time and frequency domain. Further analysis of the received signal can reveal more information about the target vehicle of interest.

Since the two world wars, radar systems have been developed, improved, and have made their way into diverse applications such as meteorology [1,2], air traffic control [3,4], structural health monitoring [5,6], synthetic aperture imaging [7,8], and underwater sensing [9,10], among others. The unwanted echoes of the transmit signal that are received as delayed and frequency-shifted versions of the transmitted signal and are correlated with the main backscattered signal from the target of interest are generally referred to as clutter. Furthermore, noise is the term usually used for signal-independent interference such as effects of adverse jamming signals [11] as well as thermal noise and atmospheric disturbances. Note that both clutter and noise degrade the accuracy of target parameter estimation; thus, making the receive filter heavily dependent not only on the transmit signal but interference as well. Since the concept of cognitive radar was first introduced by [12] in 2006, it has gained significant interest among researchers for its superior performance in resolving target parameters. According to [12], a cognitive radar *"continuously learns about the environment through experience gained from interactions with the environment, the transmitter adjusts its illumination of the environment in an intelligent manner, the whole radar system constitutes a dynamic closed feedback loop encompassing the transmitter, environment, and receiver."* A judicious design of cognitive radar where both the transmit signal and the receive filter are optimized in a joint manner can consequently lead to a more accurate estimation of the target parameters and a more tractable computational cost for the radar system.

One immediate and well-known choice for the receive filter would be the matched filter (MF) that maximizes the signal-to-noise ratio (SNR) in the presence of additive white noise. The MF multiplies the received signal with a mirrored and delayed image of the transmitted signal [11]. By locating the peak of the output signal, MF discovers the time delay of the received signal, which facilitates the estimation of the distance of the target from the radar, otherwise known as the range. On the other hand, a relative difference in motion between the target and the radar results in a Doppler frequency shift in the received signal spectrum. In the case of a perceivable Doppler shift in the received signal, a bank of MFs is adopted to estimate the Doppler shift, where the critical frequency of each MF is tuned to a different Doppler frequency [13]. However, MF performs poorly in the presence of interference with arbitrary covariance in the received signal [14]. Such limitations of MF have led researchers to search for new avenues to suppress interference/clutter. For instance, a simple solution can be to minimize the autocorrelation sidelobes of the transmit signal [15–17] along with designing the corresponding MF for the receiver. Another line of research can be found in [18–21] where the effects of the clutter are mitigated by minimizing the sidelobes of an ambiguity function (AF). In addition, the negative effects of interference, especially due to jamming, can be avoided by putting little energy of the transmit signal into the frequency bands where the presence of jamming is significant. Furthermore,

different hardware constraints such as maximum clipping of power amplifiers and analog-to-digital converters (ADC) decrease the performance of MF estimation.

For a more efficient estimation of the target parameters, one can aim to maximize the signal-to-clutter-plus-interference ratio (SCIR) in lieu of SNR. Such a scenario arises when the target detection performance of the radar is deteriorated by clutter or jamming. In such cases, one can use a mismatched filter (MMF) instead of an MF [22]. An MMF is basically a pulse compression approach where the filter is not perfectly *matched* to the expected received signal but rather is *matched* to an altered time function [23]. In comparison with the MF, an MMF allows more degrees of freedom by introducing a receive filter that performs as well as or possibly better than the MF in most clutter conditions. Furthermore, the formulation of MMF is not subject to different practical power constraints of the transmit signals such as constant-modulus (CM) constraint, similarity constraint (SC), and low peak-to-average power ratio (PAPR). Hence, a joint design of the transmit signal and the MMF receive filter can offer a more robust parameter estimation framework.

The quest for jointly designing radar sequences and corresponding receive filters for clutter/interference rejection has been longstanding among researchers [14,22,24–30]. In [24], the authors presented a joint design scheme of the transmit waveform and receive filter by minimizing the mean-square error (MSE) of the estimate of a target's scattering coefficient in the presence of clutter and interference subject to some of the practical constraints mentioned earlier. In particular, they presented three flavors of their algorithm: Cognitive REceiver and Waveform design (CREW); namely, CREW (gra), CREW (fre), and CREW (mat) based on how they seek to optimize their problem objective. The CREW (gra) algorithm uses a gradient-based approach to minimize the MSE that stems from using the optimum MMF. On the other hand, the CREW (fre) transforms the objective into the frequency domain and focuses on obtaining an optimum power spectrum for the transmit sequence. They further showed that the CREW (fre) algorithm can be specialized to the MF case and, thus, provided a new algorithm called CREW (mat) which can be viewed as an extension of the cyclic algorithms presented in [15]. Another variation of CREW, namely, CREW (cyclic), can be found in [14], where the authors formulated a cyclic approach to jointly design the transmit waveform and receive filter coefficients. For more on this topic, see [14] and the references within.

It is important to note that sampling and quantization of the signal of interest is the first step in digital signal processing. The analog-to-digital conversion ideally requires an infinite number of bits to identically represent the original analog signal, which is not feasible in practice. In fact, the aforementioned techniques assume that the received signal is available in full precision. The resulting error of quantization can then be modeled as additive noise that usually has little to no impact on algorithms that assume the infinite precision case, provided that the sampling resolution is high enough [31]. The signals of interest in many modern applications, albeit, are extremely wideband and may pass through several RF chains that require multitudinous uses of ADCs. Such modern applications include spectral sensing for cognitive radio [32,33], cognitive radars [33], radio astronomy [34], automotive short-range radars [35], and driver assistant systems [36], to name a few.

The assumption of high-precision data is, however, not appropriate when the measurements are extremely quantized to very low bit rates. Note that the cost and the power consumption of ADCs grow exponentially with their number of quantization bits and sampling rate [37]. Such issues can be mitigated by a reduction in the number of quantization bits. In the most extreme case, the sampling process is carried out by utilizing only *one bit per sample*. This can be achieved by repeatedly comparing the signal of interest with a time-varying threshold (reference) level. On the plus side, one-bit comparators can provide an extremely high sampling rate and are very cheap and easy to manufacture [37]. Moreover, the one-bit ADCs operate on very low power, and they can significantly reduce the data flow in the system, which further reduces the overall energy consumption. One-bit sampling has been studied from a classical statistical signal processing viewpoint in [38–45], a compressive sensing viewpoint in [46–50], and a sampling and reconstruction viewpoint in [51,52]. It has been shown in [46–49] that under certain assumptions, with enough one-bit samples, one can recover the full-precision data with bounded error. Further, note that in many recent works, one-bit ADCs on the receiver side are shown to be quite efficient in resolving target parameters when accompanied by suitable one-bit digital-to-analog converters (DACs) on the transmit side [53].

In this chapter, we focus on the radar processing and parameter estimation schemes for both stationary and moving targets using one-bit samplers with time-varying thresholds. For both cases of stationary and moving targets, we provide an approach that is formulated as minimization of a multivariate weighted least-squares objective with linear constraints that can be solved in an iterative manner [54]. As stated earlier, the mentioned approach is cost-effective and computationally efficient. Moreover, one-bit radar covariance estimation will be discussed.

The rest of this chapter is organized as follows. In Section 13.2, we discuss and formulate the estimation problem in the case of a stationary target. Section 13.3 describes a state-of-the-art approach to recover target parameters based on the *Bussgang theorem*. The radar algorithm to estimate the aforementioned parameters is presented in Section 13.4 for a stationary target. In Section 13.5, we extend the problem formulation, as well as the estimation algorithm, for parameter estimation in moving target scenarios. We further extend the parameter estimation formulations for a stationary target scenario to more advanced setups in Section 13.6. Numerical results that verify the validity of claims and examine the performance of the proposed algorithms are presented in Section 13.7. One-bit radar waveform and receive filter design is discussed in Section 13.8, followed by relevant numerical investigations in Section 13.9. Finally, Section 13.10 concludes the chapter.

Notation: We use bold lowercase letters for vectors and bold uppercase letters for matrices. x_i denotes the ith component of the vector $\mathbf{x}$. $(\cdot)^T$ and $(\cdot)^H$ denote the transpose and the conjugate transpose of the vector or matrix argument, respectively. $(\cdot)^*$ denotes the complex conjugate of a complex matrix, vector, or scalar. $\|\cdot\|$ denotes the l_2 norm of a vector, while $\|\cdot\|_F$ denotes the Frobenius norm of a matrix. $\Re(\cdot)$ and $\Im(\cdot)$ are the real and imaginary parts of a complex vector or scalar, respectively. Furthermore, the sets of real, complex, and natural numbers are denoted by $\mathbb{R}$, $\mathbb{C}$, and $\mathbb{N}$, respectively. $\text{sgn}(\cdot)$ is the element-wise sign operator with an output of $+1$

for non-negative numbers and -1 otherwise. Moreover, tr $(\cdot)$ and $\mathcal{N}(\cdot)$ represent the trace and the normalization operator on a matrix argument. **I** is the identity matrix. In addition, diag $(\cdot)$ and Diag $(\cdot)$ represent the diagonal vector of its argument matrix and the diagonal matrix made with its argument vector, respectively. $\mathbb{E}\{\cdot\}$ and Cov$(\cdot)$ denote the expectation and the covariance operator, respectively. Finally, the symbol $\odot$ represents the Hadamard product of matrices.

13.2 System model

Let

$$\mathbf{s} = \begin{bmatrix} s_1 & s_2 & \dots & s_N \end{bmatrix}^T \in \mathbb{C}^N \tag{13.1}$$

denotes the complex-valued radar transmit sequence of length N that will be used to modulate a train of subpulses [13]. The energy of $\{s_k\}_{k=1}^N$ is constrained to be N:

$$\|\mathbf{s}\|^2 = N \tag{13.2}$$

without any loss of generality. We shall first adopt the discrete data model described in [24,55] in order to lay out the problem formulation for the simpler case of non-moving targets. Under the assumptions of negligible intrapulse Doppler shift and that the sampling is synchronized to the pulse rate, the received discrete-time baseband signal after pulse compression and proper alignment to the range cell of interest will satisfy the following [22,55]:

$$\begin{aligned} \mathbf{y} = \alpha_0 \begin{bmatrix} s_1 \\ \vdots \\ s_{N-1} \\ s_N \end{bmatrix} + \alpha_1 \begin{bmatrix} 0 \\ s_1 \\ \vdots \\ s_{N-1} \end{bmatrix} + \cdots + \alpha_{N-1} \begin{bmatrix} 0 \\ \vdots \\ 0 \\ s_1 \end{bmatrix} \\ + \alpha_{-1} \begin{bmatrix} s_2 \\ \vdots \\ s_N \\ 0 \end{bmatrix} + \cdots + \alpha_{-N+1} \begin{bmatrix} s_N \\ 0 \\ \vdots \\ 0 \end{bmatrix} + \boldsymbol{\varepsilon} \end{aligned} \tag{13.3}$$

where $\alpha_0 \in \mathbb{C}$ is the scattering coefficient of the current range cell, $\{\alpha_k\}_{k\neq 0}$ are the scattering coefficients of the adjacent range cells that contribute to the clutter in $\mathbf{y}$, and $\boldsymbol{\varepsilon}$ is the signal-independent noise which comprises of measurement noise as well as other disturbances such as jamming. By collecting all the delayed samples of the transmitted signal into a matrix, the data model in (13.3) can be simplified as

$$\mathbf{y} = \mathbf{A}^H \boldsymbol{\alpha} + \boldsymbol{\varepsilon} \tag{13.4}$$

where

$$\mathbf{A}^H = \begin{bmatrix} s_1 & 0 & \dots & 0 & s_N & s_{N-1} & \dots & s_2 \\ s_2 & s_1 & \dots & \vdots & 0 & s_N & \dots & \vdots \\ \vdots & \vdots & \ddots & 0 & \vdots & \vdots & \ddots & s_N \\ s_N & s_{N-1} & \dots & s_1 & 0 & 0 & \dots & 0 \end{bmatrix}, \tag{13.5}$$

and

$$\boldsymbol{\alpha} = \begin{bmatrix} \alpha_0 \, \alpha_1 \, \dots \, \alpha_{N-1} \, \alpha_{-(N-1)} \, \dots \, \alpha_{-1} \end{bmatrix}^T \tag{13.6}$$

is the corresponding scattering coefficient vector. In (13.5), the first column of $\mathbf{A}^H$ represents the principal reflection from the target after range cell alignment, and the columns from the second to the last of $\mathbf{A}^H$ are, in fact, the different delayed echos of the transmit signal $\mathbf{s}$ (see [55] for more details). Furthermore, if the Doppler shifts are not negligible due to the relative difference in motion between the target and the radar system, the data model in (13.4) needs to be modified to accommodate the same and has been discussed in Section 13.5.

By applying one-bit comparators at the receiver, the sampled baseband signal can be written as:

$$\begin{aligned} \boldsymbol{\gamma}_r &= \operatorname{sgn}\left(\Re\{\mathbf{A}^H\boldsymbol{\alpha} + \boldsymbol{\varepsilon} - \boldsymbol{\lambda}\}\right), \\ \boldsymbol{\gamma}_i &= \operatorname{sgn}\left(\Im\{\mathbf{A}^H\boldsymbol{\alpha} + \boldsymbol{\varepsilon} - \boldsymbol{\lambda}\}\right), \\ \boldsymbol{\gamma} &= \tfrac{1}{\sqrt{2}}(\boldsymbol{\gamma}_r + j\boldsymbol{\gamma}_i), \end{aligned} \tag{13.7}$$

where $\boldsymbol{\lambda}$ is the tunable complex-valued threshold level vector at the comparators, whose design is discussed in Section 13.4. Note that in (13.7), we sample both real and imaginary parts of the received signal in order to preserve the phase information. We further assume that the clutter coefficients $\{\alpha_k\}_{k\neq 0}$ are zero-mean and their variance,

$$\beta \triangleq \mathbb{E}\{|\alpha_k|^2\}, \qquad k \neq 0, \tag{13.8}$$

and the covariance matrix of $\boldsymbol{\varepsilon}$,

$$\boldsymbol{\Gamma} \triangleq \mathbb{E}\{\boldsymbol{\varepsilon}\boldsymbol{\varepsilon}^H\}, \tag{13.9}$$

are known quantities. We further assume that $\{\alpha_k\}_{k\neq 0}$ are independent of each other and of $\boldsymbol{\varepsilon}$ as well. Note that, in radar applications, both $\boldsymbol{\Gamma}$ and β can be acquired using various preprocessing techniques, *e.g.*, by employing pre-scans, and are typically assumed to be known *a priori* [24]. A detailed discussion of the pre-scanning process can be found in [12].

As mentioned earlier, once the received signal $\mathbf{y}$ is available, one can estimate the target backscattering coefficient α_0 by exploiting the signal model in (13.4) using an MMF. The MMF estimate of α_0 has the following linear form in $\mathbf{y}$ [14]:

$$\hat{\alpha}_0 = \frac{\mathbf{w}^H\mathbf{y}}{\mathbf{w}^H\mathbf{s}} \tag{13.10}$$

where $\mathbf{w} \in \mathbb{C}^N$ is the MMF vector of the receive filter. The MSE of the mentioned estimate can be derived as

$$\mathrm{MSE}(\hat{\alpha}_0) = \mathbb{E}\left\{\left|\frac{\mathbf{w}^H\mathbf{y}}{\mathbf{w}^H\mathbf{s}} - \alpha_0\right|^2\right\} = \frac{\mathbf{w}^H\mathbf{R}\mathbf{w}}{\left|\mathbf{w}^H\mathbf{s}\right|^2} \tag{13.11}$$

where

$$\mathbf{R} = \beta \sum_{0<|k|\leq(N-1)} \mathbf{J}_k \mathbf{s}\mathbf{s}^H \mathbf{J}_k^H + \mathbf{\Gamma}, \tag{13.12}$$

is the covariance matrix of the interference terms in (13.4), and $\{\mathbf{J}_k\}$ are the shift matrices formulated as

$$\mathbf{J}_k = \mathbf{J}_{-k}^H = \begin{bmatrix} 0 & \dots & 0 & 1 & \dots & 0 \\ \vdots & & & & \ddots & \\ & & & & & 1 \\ \underbrace{0 \dots 0}_{k} & \dots & & & & \end{bmatrix}^H_{N\times N}, \qquad k = 0, 1, \cdots, N-1. \tag{13.13}$$

Note that the denominator of the MSE in (13.11) is the power of the signal at the receiver, and its numerator is the power of the interferences. Therefore, minimizing the MSE is identical to maximizing the SCIR.

Note that one can exploit the relationship between the covariance matrices of the received signals before and after the non-linear transformation of one-bit sampling in order to estimate the target parameter α_0. This relationship is provided by the Bussgang theorem in a *normalized* sense where the interference is assumed to be Gaussian in nature [56]. In the following section, we briefly discuss a state-of-the-art Bussgang-theorem-aided procedure to estimate α_0. Afterward, in Section 13.4, we present an algorithm that, through minimizing the MSE, jointly recovers the scattering coefficient of the current range cell, α_0, and the received signal, $\mathbf{y}$, from the one-bit sampled received data $\boldsymbol{\gamma}$, as introduced in (13.7).

13.3 Bussgang-theorem-aided estimation

In this section, we describe a state-of-the-art Bussgang-theorem-aided approach to estimate the target parameters [56]. Let $Y(t)$ be a real-valued, scalar, and stationary Gaussian process that undergoes the one-bit sampling process $Z(t) = \mathrm{sgn}(Y(t))$. The autocorrelation function of the process $Z(t)$, denoted by $R_Z(\tau)$, is given by

$$R_Z(\tau) = \mathbb{E}\{Z(t+\tau)Z(t)\} = \frac{2}{\pi}\sin^{-1}\left(\bar{R}_Y(\tau)\right) \tag{13.14}$$

where $\bar{R}_Y(\tau) = R_Y(\tau)/R_Y(0)$ is the normalized autocorrelation function of the process $Y(t)$ [57]. The good news is that the Bussgang theorem [56] states that the cross-correlation function of the processes $Y(t)$ and $Z(t)$ is proportional to the autocorrelation function of $Y(t)$, *i.e.*, $R_{ZY}(\tau) = \mu R_Y(\tau)$, where the factor μ depends on the power of the process $Y(t)$.

The case of complex-valued vector processes, which was studied in [58], can be extended in a similar manner. Let $\mathbf{y}$ be the complex-valued vector whose one-bit samples are given by $\boldsymbol{\gamma} = \frac{1}{\sqrt{2}}\left(\text{sgn}(\Re(\mathbf{y})) + j\text{sgn}(\Im(\mathbf{y}))\right)$, as in (13.7). Then the normalized autocorrelation of the vector $\mathbf{y}$ is given by

$$\bar{\mathbf{R}}_{\mathbf{y}} = \mathcal{N}(\mathbf{R}_{\mathbf{y}}) \triangleq \mathbf{D}^{-1/2}\mathbf{R}_{\mathbf{y}}\mathbf{D}^{-1/2} \tag{13.15}$$

where $\mathbf{D} = \mathbf{R}_{\mathbf{y}} \odot \mathbf{I}$ is a diagonal matrix containing only the diagonal entries of $\mathbf{R}_{\mathbf{y}}$. It has been shown in [58] that the following covariance equality holds:

$$\bar{\mathbf{R}}_{\mathbf{y}} = \sin\left(\frac{\pi}{2}\mathbf{R}_{\boldsymbol{\gamma}}\right), \tag{13.16}$$

where $\mathbf{R}_{\boldsymbol{\gamma}}$ is the autocorrelation matrix of the one-bit sampled data, $\boldsymbol{\gamma}$.

In order to apply the above results to the one-bit radar processing problem using a threshold level vector $\boldsymbol{\lambda} \in \mathbb{C}^N$, we can derive the covariance matrix of the difference between the received signal and the time-varying threshold, viz.

$$\mathbf{R}_{\mathbf{y}-\boldsymbol{\lambda}} = |\alpha_0|^2\mathbf{s}\mathbf{s}^H + \boldsymbol{\lambda}\boldsymbol{\lambda}^H + \mathbf{R} - 2\Re(\alpha_0\mathbf{s}\boldsymbol{\lambda}^H). \tag{13.17}$$

Therefore, one can compute the scattering coefficient α_0 by solving the following non-convex optimization problem:

$$\min_{\alpha_0} \quad \left\|\bar{\mathbf{R}}_{\mathbf{y}-\boldsymbol{\lambda}} - \mathcal{N}(|\alpha_0|^2\mathbf{s}\mathbf{s}^H + \boldsymbol{\lambda}\boldsymbol{\lambda}^H + \mathbf{R} - 2\Re(\alpha_0\mathbf{s}\boldsymbol{\lambda}^H))\right\|_F \tag{13.18}$$

in which $\bar{\mathbf{R}}_{\mathbf{y}-\boldsymbol{\lambda}}$ is obtained via (13.16), and using only one observation or *snapshot* of $\boldsymbol{\gamma}$.

13.4 Radar processing for stationary targets

In this section, we discuss the proposed approach to recover both the received signal $\mathbf{y}$ and the scattering coefficient α_0 from the one-bit sampled received signal $\boldsymbol{\gamma}$ for a stationary target by minimizing the aforementioned MSE in (13.11).

For a given transmit sequence $\mathbf{s}$, the optimum receive filter $\mathbf{w}$ can be simply given as closed-form solution [14,24]:

$$\mathbf{w} = \mathbf{R}^{-1}\mathbf{s} \tag{13.19}$$

up to a multiplicative constant. Nevertheless, the MMF approach to recover α_0, discussed in (13.10), requires the availability of the un-quantized (or high-resolution quantized) received signal $\mathbf{y}$, which is unfortunately not available directly due to the one-bit sampling of the received signal. Therefore, we shall resort to an alternative optimization approach that utilizes the one-bit sampled data $\boldsymbol{\gamma}$ in lieu of $\mathbf{y}$ in order to estimate the target parameter. In pursuance of radar parameter recovery using one-bit sampled data with time-varying thresholds, we analyze two matters of major significance:

1. The recovery of $\mathbf{y}$ and estimation of α_0 by employing the one-bit data procured at the receiver.
2. The design of the next set of thresholds to be used at the one-bit ADCs.

13.4.1 Estimation of stationary target parameters

In order to efficiently estimate the received signal $\mathbf{y}$ and target parameter α_0, we consider minimizing the following weighted-least-squares (WLS) objective in a more generalized sense:

$$Q(\mathbf{y}, \alpha_0) \triangleq (\mathbf{y} - \alpha_0 \mathbf{s})^H \mathbf{R}^{-1} (\mathbf{y} - \alpha_0 \mathbf{s}). \tag{13.20}$$

It should be noted that the usage of the above criterion has the following advantages:

1. Unlike the MMF in (13.10), Q does not require a knowledge of $\mathbf{y}$.
2. It is a function of both $\mathbf{y}$ and α_0, laying the ground for their respective joint recovery.
3. It can easily be observed that, for any given $\mathbf{y}$, the optimum α_0 in (13.20) is identical to that of MMF in (13.10) with the use of (13.19)—thus, making it a natural choice for parameter recovery.
4. In effect, the minimization of (13.20) enforces the system model introduced in (13.3). Note that the model mismatch can be written as

$$\mathbf{y} - \alpha_0 \mathbf{s} = \tilde{\mathbf{A}}^H \tilde{\boldsymbol{\alpha}} + \boldsymbol{\varepsilon} \tag{13.21}$$

where $\tilde{\mathbf{A}}^H$ and $\tilde{\boldsymbol{\alpha}}$ are derived from $\mathbf{A}^H$ and $\boldsymbol{\alpha}$ with their first column and first entry dropped, respectively. It can easily be established that the objective function in (13.20) penalizes the model mismatch based on the second-order mismatch statistics derived as

$$\begin{aligned} &\mathbb{E}\left\{\left(\tilde{\mathbf{A}}^H \tilde{\boldsymbol{\alpha}} + \boldsymbol{\varepsilon}\right)\left(\tilde{\mathbf{A}}^H \tilde{\boldsymbol{\alpha}} + \boldsymbol{\varepsilon}\right)^H\right\} \\ &= \mathbb{E}\left\{\tilde{\mathbf{A}}^H \tilde{\boldsymbol{\alpha}} \tilde{\boldsymbol{\alpha}}^H \tilde{\mathbf{A}}\right\} + \mathbb{E}\left\{\boldsymbol{\varepsilon}\boldsymbol{\varepsilon}^H\right\} \\ &= \mathbf{R}. \end{aligned} \tag{13.22}$$

Hence, based on the property 3, and by substituting the optimum α_0, the objective function (13.20) can be reformulated as

$$\begin{aligned} Q(\mathbf{y}, \hat{\alpha}_0) &\triangleq Q(\mathbf{y}) \\ &= \mathbf{y}^H \left(\mathbf{I} - \frac{\mathbf{s}\mathbf{w}^H}{\mathbf{w}^H \mathbf{s}}\right)^H \mathbf{R}^{-1} \left(\mathbf{I} - \frac{\mathbf{s}\mathbf{w}^H}{\mathbf{w}^H \mathbf{s}}\right) \mathbf{y}. \end{aligned} \tag{13.23}$$

Hence, the problem of jointly estimating α_0 and $\mathbf{y}$ boils down to:

$$\begin{aligned} \min_{\mathbf{y}} \quad & \mathbf{y}^H \left[\left(\mathbf{I} - \frac{\mathbf{s}\mathbf{w}^H}{\mathbf{w}^H \mathbf{s}}\right)^H \mathbf{R}^{-1} \left(\mathbf{I} - \frac{\mathbf{s}\mathbf{w}^H}{\mathbf{w}^H \mathbf{s}}\right)\right] \mathbf{y} \\ \text{s.t.} \quad & \boldsymbol{\Omega}_r (\mathbf{y}_r - \boldsymbol{\lambda}_r) \geq \mathbf{0}, \\ & \boldsymbol{\Omega}_i (\mathbf{y}_i - \boldsymbol{\lambda}_i) \geq \mathbf{0}, \end{aligned} \tag{13.24}$$

where $(\mathbf{y}_r, \mathbf{y}_i)$ and $(\boldsymbol{\lambda}_r, \boldsymbol{\lambda}_i)$ denote the real and imaginary parts of $\mathbf{y}$ and $\boldsymbol{\lambda}$, respectively, and $\boldsymbol{\Omega}_r \triangleq \text{Diag}\left(\boldsymbol{\gamma}_r\right)$, $\boldsymbol{\Omega}_i \triangleq \text{Diag}\left(\boldsymbol{\gamma}_i\right)$. One can easily verify that the optimization problem in (13.24) is a convex quadratic program with linear constraints that can be

Algorithm 1: One-bit radar parameter estimation for stationary targets

Ensure: The transmit sequence $\mathbf{s}$ and set the threshold vector $\boldsymbol{\lambda}$ arbitrarily, or generate according to (13.25) and (13.26).

1: Compute the optimal MMF vector $\mathbf{w}$ using (13.19).
2: Compute the optimal vector $\mathbf{y}$ by solving (13.24).
3: Estimate the target scattering coefficient α_0 using the MMF estimator in (13.10).
4: In case of tracking, set $\boldsymbol{\lambda}$ according to (13.25) and (13.26) and go to Step 2.

solved efficiently. Upon finding the optimal $\mathbf{y}$, the optimal α_0 can be calculated using the MMF estimate in (13.10).

It is worth noting that the optimization problem in (13.24) can easily be translated into a non-negative least-squares (NNLS) optimization problem. This can be achieved by changing variables such that $\tilde{\mathbf{y}}_r \triangleq \boldsymbol{\Omega}_r (\mathbf{y}_r - \boldsymbol{\lambda}_r)$ and $\tilde{\mathbf{y}}_i \triangleq \boldsymbol{\Omega}_i (\mathbf{y}_i - \boldsymbol{\lambda}_i)$, adding up to $\tilde{\mathbf{y}} \triangleq \tilde{\mathbf{y}}_r + j\tilde{\mathbf{y}}_i$. As a result, fast NNLS approaches can be exploited to expedite the recovery process [59].

13.4.2 Time-varying threshold design

In the following, we briefly discuss how one can choose the threshold vector $\boldsymbol{\lambda}$ depending on the number of one-bit ADCs being used on the receiver side.

13.4.2.1 Sampling with a single one-bit ADC

From an information-theoretic viewpoint, in order to collect the *most* information on $\mathbf{y}$, one could expect $\boldsymbol{\lambda}$ to be set in such a way that by considering the *a priori* information, observing any of the two outcomes in the set $\{-1, +1\}$ at the output of the one-bit sampler for a single sample has the same likelihood. In a general case, $\boldsymbol{\lambda}$ is expected to partition the set of likely events into subsets with similar *cardinality*. When the probability density function (pdf) of the received signal follows a Gaussian distribution, this goal is achieved by setting $\boldsymbol{\lambda}$ as close as possible to the expected value of $\mathbf{y}$. More precisely, we choose:

$$\boldsymbol{\lambda} = \mathbb{E}\{\alpha_0\}\,\mathbf{s}. \tag{13.25}$$

In other words, the choice of $\boldsymbol{\lambda}$ will be governed by our *future* expectation of the value of α_0. This is particularly pertinent to target-tracking scenarios.

13.4.2.2 Sampling with multiple one-bit ADCs

We note that our estimation method can easily be extended to cases where the signal is sampled by several ADCs in parallel. This only leads to extra linear constraints in (13.24). Assuming that K number of ADCs is used, and the thresholds are set *a priori*, in the single sample case, the thresholds are optimal if they partition the set of likely events into $K + 1$ subsets with similar *cardinality*. The determination of the thresholds will be even more difficult when the number of samples or the number of ADCs grows large. However, a close *approximation* of the optimal threshold vectors

$\{\boldsymbol{\lambda}_k\}_{k=1}^K$ can be obtained by assuming $\{\boldsymbol{\lambda}_k\}_{k=1}^K$ to be random variables [37]. In other words, a good set of random sampling threshold vectors $\{\boldsymbol{\lambda}_k\}_{k=1}^K$ should mimic the behavior of $\mathbf{y}$. In particular, we generate $\{\boldsymbol{\lambda}_k\}_{k=1}^K$ as a set of random vectors similar to $\mathbf{y}$ that has the same (Gaussian) distribution:

$$\begin{aligned} \mathbb{E}\{\boldsymbol{\lambda}\} &= \mathbb{E}\{\alpha_0\}\,\mathbf{s}, \\ \mathrm{Cov}(\boldsymbol{\lambda}) &= \mathbb{E}\left\{|\alpha_0|^2\right\}\,\mathbf{s}\mathbf{s}^H + \mathbf{R}. \end{aligned} \tag{13.26}$$

The steps of the proposed approach are summarized in Algorithm 1 for reader's convenience.

13.5 Radar processing for moving targets

In this section, we consider the moving targets scenario where the Doppler effect can no longer be neglected. In order to perform a recovery of radar parameters, *i.e.*, the backscattering coefficient and the Doppler shift of the target, we first update the system model of (13.3) and then modify the proposed approach discussed in Section 13.4 to recover the normalized Doppler shift as well.

13.5.1 Problem formulation for moving targets

Let $\mathbf{s} \in \mathbb{C}^N$ denote the discrete-time transmit sequence of a digital system, as in (13.1). After alignment to the range-azimuth cell of interest, the new discrete-time complex-valued received baseband data vector, which is backscattered from the moving target in the corresponding range-azimuth cell, can be formulated as (see [30,60–62])

$$\mathbf{y} = \alpha_0(\mathbf{s} \odot \mathbf{p}(\nu)) + \mathbf{c} + \mathbf{n}, \tag{13.27}$$

where α_0 is the complex backscattering coefficient of the target in the current range-azimuth cell and $\mathbf{p}(\nu) = \left[e^{j2\pi(0)\nu},\ e^{j2\pi(1)\nu},\ \ldots,\ e^{j2\pi(N-1)\nu}\right]^T$ is the propagation effect vector with $\nu \in [-0.5, 0.5)$ being the normalized Doppler shift of the target. The N-dimensional vectors $\mathbf{c}$ and $\mathbf{n}$ denote the signal-dependent clutter and signal-independent noise, respectively. The clutter vector $\mathbf{c}$ is comprised of returned echos from uncorrelated scatterers at different range-azimuth cells [62] (as depicted in Figure 13.1), which are spread in Doppler frequency due to the possible clutter motion and can be formulated as

$$\mathbf{c} = \sum_{k=0}^{N_c-1} \sum_{l=0}^{L-1} \alpha_{(k,l)} \mathbf{J}_k \left[\mathbf{s} \odot \mathbf{p}(\nu_{d_{(k,l)}})\right], \tag{13.28}$$

where $N_c \leq N$ is the number of range-rings, L is the number of various azimuth sectors, and $\alpha_{(k,l)}$ and $\nu_{d_{(k,l)}}$ are the scattering coefficient and normalized Doppler shift of the (k,l)-th range-azimuth cell, respectively, interfering with the range-azimuth cell of interest. The matrix $\mathbf{J}_k$ is defined in the same way as in (13.13).

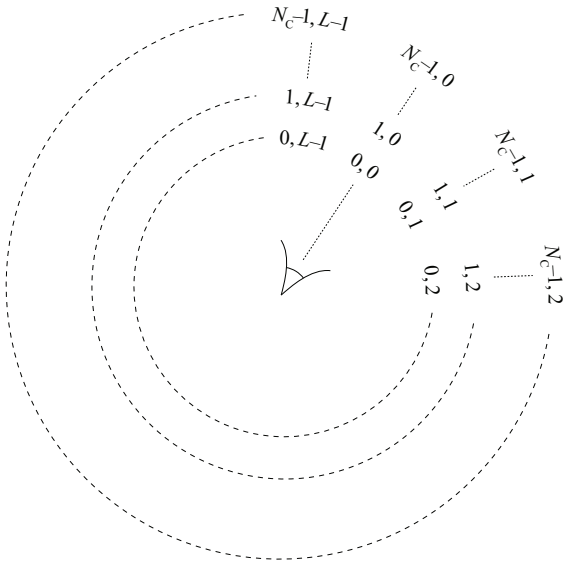

Figure 13.1 The setting for different range-azimuth cells. All the cell numbers are shown in (range, azimuth) pairs.

The covariance matrix of the clutter vector $\mathbf{c}$ can be written as

$$\mathbf{\Sigma_c} = \sum_{k=0}^{N_c-1} \sum_{l=0}^{L-1} \sigma^2_{(k,l)} \mathbf{J}_k \mathbf{\Phi}\left(s,(k,l)\right) \mathbf{J}_k^T \tag{13.29}$$

with $\sigma^2_{(k,l)}$ being the average scattering power of the scatterer in (k,l)-th range-azimuth cell. Furthermore, $\mathbf{\Phi}$ in (13.29) can be expressed as

$$\mathbf{\Phi}\left(s,(k,l)\right) = \text{Diag}\left(\mathbf{s}\right) \mathbf{C}_v(k,l) \text{Diag}\left(\mathbf{s}\right)^H,$$

where $\mathbf{C}_v(k,l)$ is the covariance matrix of the propagation effect vector of the (k,l)th cell [62], defined as

$$\mathbf{C}_v(k,l) = \begin{cases} 1 & k = l \\ e^{j(k-l)\bar{\nu}_{d_{(k,l)}}} \dfrac{\sin\left(\frac{k-l}{2}\varepsilon_{d_{(k,l)}}\right)}{\sin\left(\frac{k-l}{2}\varepsilon_{d_{(k,l)}}\right)} & k \neq l. \end{cases} \tag{13.30}$$

Similar to (13.9), we denote the covariance matrix of the signal-independent interference by $\mathbf{\Gamma}$, and re-define the covariance matrix of the interference as follows:

$$\mathbf{R} = \text{Cov}(\mathbf{c} + \mathbf{n}) = \mathbf{\Sigma_c} + \mathbf{\Gamma}. \tag{13.31}$$

Moreover, in (13.29), the clutter patches in each range-azimuth cell are assumed to have uniform Doppler shifts in the interval $\Omega_c = \left(\bar{\nu}_{d_{(k,l)}} - \frac{\varepsilon_{d_{(k,l)}}}{2}, \bar{\nu}_{d_{(k,l)}} + \frac{\varepsilon_{d_{(k,l)}}}{2}\right)$ [61]. Note that the assumption of having uniform Doppler shifts in each range-azimuth cell

Algorithm 2: One-bit radar parameter estimation for moving targets

Ensure: The transmit sequence $\mathbf{s}$ and set the threshold vector $\boldsymbol{\lambda}$ arbitrarily or generate according to (13.40).

1: For fixed $\mathbf{y}$, α_0, and ν, compute the optimal MMF vector $\mathbf{w}$ according to (13.33).
2: For fixed $\mathbf{w}$ and ν, compute the optimal vector $\mathbf{y}$ by solving the criterion in (13.35) with respect to $\mathbf{y}$.
3: For fixed $\mathbf{y}$ and $\mathbf{w}$, compute the optimal target normalized Doppler shift ν by minimizing the criterion in (13.37).
4: If convergence is reached, go to Step 5; otherwise, go to Step 1.
5: For fixed $\mathbf{w}$, $\mathbf{y}$, and ν, estimate the target backscattering coefficient α_0 using (13.32).
6: In case of tracking, set $\boldsymbol{\lambda}$ according to (13.40) and go to Step 1.

results from the fact that the clutter patches in these cells can be any object in our environment, with some of them moving. If such objects are moving, even slightly, the echoes reflected from the corresponding cells will have a Doppler shift associated with that movement. Examples of such objects include vehicles, ocean waves, and trees with moving leaves due to the wind [63,64]. These contribute to a small Doppler frequency shift in clutter input which is assumed to be distributed uniformly.

13.5.2 Estimation of moving target parameters

When the received signal is available, and the Doppler shift is known, an estimation of the backscattering coefficient α_0 with minimal MSE can be achieved by using an MMF, in a similar manner as in (13.10). The estimate of the target backscattering coefficient given by MMF is

$$\hat{\alpha}_0 = \frac{\mathbf{w}^H \mathbf{y}}{\mathbf{w}^H \left(\mathbf{s} \odot \mathbf{p}(\nu)\right)}. \tag{13.32}$$

Additionally, it can be verified that the optimal $\mathbf{w}$ that minimizes the MSE criterion is given by

$$\mathbf{w} = \mathbf{R}^{-1} \left(\mathbf{s} \odot \mathbf{p}(\nu)\right). \tag{13.33}$$

up to a multiplicative constant.

Note once again that, due to using one-bit ADCs, the access to the received signal $\mathbf{y}$ is restricted to only its one-bit samples, given by (13.7). In order to tackle the problem of estimating the backscattering coefficient α_0 and the normalized Doppler shift ν, we form a modified version of the weighted-least-squares objective function in (13.20), in compliance with the system model defined in (13.27):

$$\tilde{Q}(\mathbf{y}, \alpha_0, \nu) \triangleq \left[\mathbf{y} - \alpha_0(\mathbf{s} \odot \mathbf{p}(\nu))\right]^H \mathbf{R}^{-1} \left[\mathbf{y} - \alpha_0(\mathbf{s} \odot \mathbf{p}(\nu))\right] \tag{13.34}$$

with $\mathbf{R}$ being the covariance matrix of the interference defined in (13.31).

Similar to the stationary target case, the aforementioned objective function is chosen to have the following properties:

1. It does not rely on the knowledge of the received signal $\mathbf{y}$ and yet enforces the system model in (13.27).
2. For given $\mathbf{y}$ and ν, the optimal α_0 of (13.34) is identical to the MMF estimate of α_0 in (13.32).
3. It is a function of $\mathbf{y}$, α_0, and ν, which permits their joint estimation, and last but not least.
4. The recovery of $\mathbf{y}$ using $\tilde{Q}$ paves the way for the usage of other classical signal processing methods that rely on the knowledge of $\mathbf{y}$.

The problem of jointly estimating $\mathbf{y}$, α_0, and ν for moving target determination thus becomes

$$\begin{aligned}&\min_{\mathbf{y},\alpha_0,\nu} [\mathbf{y} - \alpha_0(\mathbf{s} \odot \mathbf{p}(\nu))]^H \mathbf{R}^{-1} [\mathbf{y} - \alpha_0(\mathbf{s} \odot \mathbf{p}(\nu))] \\ &\text{s.t.} \boldsymbol{\Omega}_r (\mathbf{y}_r - \boldsymbol{\lambda}_r) \geq \mathbf{0}, \\ &\boldsymbol{\Omega}_i (\mathbf{y}_i - \boldsymbol{\lambda}_i) \geq \mathbf{0}. \end{aligned} \tag{13.35}$$

However, by substituting the optimal α_0 in (13.32) into the objective function of (13.35), we achieve a more simplified optimization problem:

$$\begin{aligned}\min_{\mathbf{w},\mathbf{y},\nu} \quad & \left\| \mathbf{R}^{-1/2} \left(\mathbf{I} - \frac{[\mathbf{s} \odot \mathbf{p}(\nu)]\mathbf{w}^H}{\mathbf{w}^H[\mathbf{s} \odot \mathbf{p}(\nu)]} \right) \mathbf{y} \right\|_2^2 \\ \text{s.t.} \quad & \boldsymbol{\Omega}_r (\mathbf{y}_r - \boldsymbol{\lambda}_r) \geq \mathbf{0}, \\ & \boldsymbol{\Omega}_i (\mathbf{y}_i - \boldsymbol{\lambda}_i) \geq \mathbf{0}. \end{aligned} \tag{13.36}$$

In order to solve the above minimization problem, we resort to cyclic optimization over $\mathbf{w}$, $\mathbf{y}$, and ν, until convergence. The optimal $\mathbf{w}$ for fixed $\mathbf{y}$ and ν can be obtained using (13.33). Next, for fixed $\mathbf{w}$ and ν, it is easy to see that the above optimization problem is a convex linearly-constrained quadratic program with respect to $\mathbf{y}$, which can be efficiently solved. Lastly, in order to find the optimal normalized Doppler shift ν when $\mathbf{w}$ and $\mathbf{y}$ are fixed, we can rewrite the optimization problem (13.35) with respect to ν as:

$$\begin{aligned}&\min_{\nu} g(\nu) \\ &\text{s.t. } \mathbf{p}(\nu) = \left[e^{j2\pi(0)\nu} \;\; e^{j2\pi(1)\nu} \;\; \ldots \;\; e^{j2\pi(N-1)\nu} \right]^T \end{aligned} \tag{13.37}$$

where

$$g(\nu) \triangleq \begin{bmatrix} 1 \\ \mathbf{p}(\nu) \end{bmatrix}^H \begin{bmatrix} 0 & -(\hat{\alpha}_0 \mathbf{s})^T \odot (\mathbf{y}^H \mathbf{R}^{-1}) \\ -(\hat{\alpha}_0 \mathbf{s})^* \odot (\mathbf{R}^{-1}\mathbf{y}) & |\hat{\alpha}_0|^2 \mathbf{R}^{-1} \odot (\mathbf{s}\mathbf{s}^H)^* \end{bmatrix} \begin{bmatrix} 1 \\ \mathbf{p}(\nu) \end{bmatrix} \tag{13.38}$$

and where $\hat{\alpha}_0$ is calculated using (13.32).

The optimization problem in (13.37) resembles that of estimating the direction-of-arrival (DOA) in uniform linear arrays (ULAs) and can be dealt with using one

of the many algorithms for estimating the DOA—see [65] for details. We repeat the cyclic optimization procedure until a pre-defined convergence criterion is satisfied. Once the $\mathbf{w}$, $\mathbf{y}$, and ν are estimated, the backscattering coefficient α_0 can be easily retrieved via (13.32).

As to the design of the threshold vector $\boldsymbol{\lambda}$, the same arguments discussed in Section 13.4.2 hold. However, the statistics of the (Gaussian) randomly generated threshold vector $\boldsymbol{\lambda}$ change as follows:

$$\begin{aligned}\mathbb{E}\{\boldsymbol{\lambda}\} &= \mathbb{E}\{\mathbf{y}\} = \mathbb{E}\{\alpha_0\}\,(\mathbf{s} \odot \mathbb{E}\{\mathbf{p}(\nu)\}),\\ \mathrm{Cov}(\boldsymbol{\lambda}) &= \mathrm{Cov}(\mathbf{y})\\ &= \mathbb{E}\left\{|\alpha_0|^2\right\}\,(\mathbf{s}\mathbf{s}^H) \odot \mathbb{E}\{\mathbf{p}(\nu)\mathbf{p}^H(\nu)\} + \mathbf{R}.\end{aligned} \tag{13.39}$$

For readers' convenience, the steps of the proposed approach for moving target radar parameter estimation are summarized in Algorithm 2.

13.6 Other low-resolution sampling scenarios

In this section, we study the extensions of the proposed method discussed in Section 13.4 to different cases for the stationary target scenario. We further note that the same extensions can be applied to the case of the moving target as well.

13.6.1 Extension to parallel one-bit comparators

It can be noted that the problem formulation in (13.24) can be extended to the implementation of an array of K number of one-bit comparators in parallel with different time-varying thresholds, denoted by $\boldsymbol{\lambda}^{(k)}$, $k = 1, \cdots, K$. In this way, the optimization problem requires the recovered signal to comply with all the comparison information that is produced by the one-bit comparators. Thus, the constraints in (13.24) can be updated as

$$\begin{aligned}&\boldsymbol{\Omega}_r^{(k)}\left(\mathbf{y}_r - \boldsymbol{\lambda}_r^{(k)}\right) \geq \mathbf{0}, \quad \forall\, k \in \{1, \cdots, K\},\\ &\boldsymbol{\Omega}_i^{(k)}\left(\mathbf{y}_i - \boldsymbol{\lambda}_i^{(k)}\right) \geq \mathbf{0}, \quad \forall\, k \in \{1, \cdots, K\},\end{aligned} \tag{13.40}$$

where $\boldsymbol{\Omega}_r^{(k)} = \mathrm{Diag}\left(\boldsymbol{\lambda}_r^{(k)}\right)$ and $\boldsymbol{\Omega}_i^{(k)} = \mathrm{Diag}\left(\boldsymbol{\lambda}_i^{(k)}\right)$.

13.6.2 Extension to p-bit ADCs

Another alternative way to glean more information from the received signal $\mathbf{y}$ is to use multi-bit ADCs. For a generic p-bit ADC, we have $(2^p - 1) + 2$ thresholds such that $\lambda_0 < \lambda_1 < \lambda_2 < \cdots < \lambda_{2^p-1} < \lambda_{2^p}$, where we define $\lambda_0 \triangleq -\infty$ and $\lambda_{2^p} \triangleq +\infty$ for the ease of notation. Thus, each sample of the input signal can fall into any of the 2^p quantization regions, which further indicates that each input sampled data has to lie in an interval $[\lambda_k, \lambda_{k+1}]$, for some $0 \leq k \leq (2^p - 1), k \in \mathbb{N} \cup \{0\}$. Thus, if q number of p-bit ADCs are used instead of one-bit comparators, each of the ADCs will have $(2^p - 1) + 2$ thresholds—leading to a total number of $q(2^p + 1)$ thresholds.

Observe that the optimization problem in this case requires enforcing the following constraints:

$$[\mathbf{y}_r]_n \in \left[[\boldsymbol{\lambda}_r]_n^{(k_n)}, [\boldsymbol{\lambda}_r]_n^{(k_n+1)}\right],$$
$$[\mathbf{y}_i]_m \in \left[[\boldsymbol{\lambda}_i]_m^{(k_m)}, [\boldsymbol{\lambda}_i]_m^{(k_m+1)}\right],$$

for all $n, m \in \{1, \cdots, N\}$ and for integers k_n and k_m provided by the p-bit ADCs, where $[\boldsymbol{\lambda}_r]_n^{(k_n)}$ and $[\boldsymbol{\lambda}_i]_m^{(k_m)}$ denote the k_nth and k_mth components of $[\boldsymbol{\lambda}_r]_n$ and $[\boldsymbol{\lambda}_i]_m$, respectively. Let,

$$\boldsymbol{\lambda}_r^{lower} \triangleq \left[[\boldsymbol{\lambda}_r]_1^{(k_1)}, \cdots, [\boldsymbol{\lambda}_r]_N^{(k_N)}\right]^T,$$
$$\boldsymbol{\lambda}_r^{upper} \triangleq \left[[\boldsymbol{\lambda}_r]_1^{(k_1+1)}, \cdots, [\boldsymbol{\lambda}_r]_N^{(k_N+1)}\right]^T, \tag{13.41}$$

and define $\boldsymbol{\lambda}_i^{lower}$ and $\boldsymbol{\lambda}_i^{upper}$ in a similar manner. Then, the constraints of the optimization problem in (13.24) can be updated, in this case, as

$$\begin{aligned}
+1 \cdot (\mathbf{y}_r - \boldsymbol{\lambda}_r^{lower}) &\geq \mathbf{0}, \\
+1 \cdot (\mathbf{y}_i - \boldsymbol{\lambda}_i^{lower}) &\geq \mathbf{0}, \\
-1 \cdot (\mathbf{y}_r - \boldsymbol{\lambda}_r^{upper}) &\geq \mathbf{0}, \\
-1 \cdot (\mathbf{y}_i - \boldsymbol{\lambda}_i^{upper}) &\geq \mathbf{0}.
\end{aligned} \tag{13.42}$$

13.7 Numerical analysis for one-bit radar signal processing

In this section, we delve into examining the performance of the proposed target parameter estimation methods. The estimation error of our proposed approaches is compared with that of the Bussgang-aided approach of Section 13.3, and estimation using un-quantized received signal, denoted by ∞-precision. We first consider the case of stationary targets and employ the approach discussed in Section 13.4 and then move on to the case of moving targets discussed in Section 13.5.

13.7.1 Stationary targets

For the simulations, we assume that the noise is additive, white, and Gaussian with a variance of 0.1, the average clutter power β is 0.1, and that the transmit sequence is generated using the method in [14] with a PAPR of 1. The results in all cases are averaged over 100 runs of the algorithms unless mentioned otherwise.

Let $\hat{\alpha}_0$ denote the estimate of α_0, and further define the normalized estimation error as $|\alpha_0 - \hat{\alpha}_0|/|\alpha_0|$. In Figure 13.2, the normalized estimation error obtained via a Monte-Carlo method with randomly generated ground truths for α_0 is plotted against the transmit sequence length N for the proposed algorithm, the Bussgang-aided approach of Section 13.3, and the $\infty - precision$ case. In addition, for visualization, Figure 13.3 shows the results of the estimations, in the Monte-Carlo method for $\alpha_0 = (0.5 + j0.5)$ for $N \in \{50, 100, 1,000\}$ on the complex plane. It can be seen from

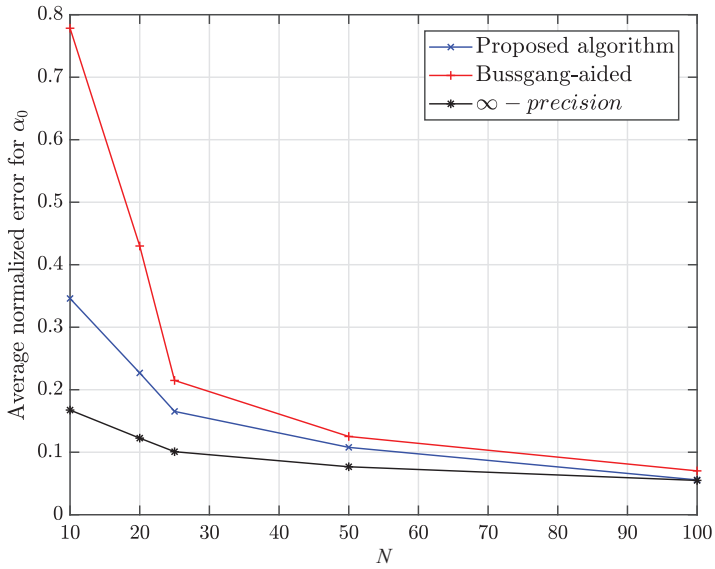

Figure 13.2 Average normalized estimation error of stationary target scattering coefficient α_0, defined by the ratio $|\alpha_0 - \hat{\alpha}_0|/|\alpha_0|$, for different transmit sequence lengths $N \in \{10, 25, 50, 100\}$

both figures that the estimate of the proposed algorithm approaches that of the ∞-precision as N grows large. This is expected because when N grows large, the number of comparisons grows large at the same rate revealing the true nature of the unquantized data. From an information-theoretic point of view, this translates to more available information on the received signal through its one-bit samples that contribute to the amelioration of the scattering coefficient recovery. Consequently, the estimation performances of all three approaches are enhanced with an increase of N, as is apparent in both figures.

Figure 13.4 shows the performance of the proposed algorithm in the presence of different noise power levels for the stationary target and compares it with that of $\infty - precision$ case. For this experiment, we keep $N = 25$, and again assume that the noise is additive, white, and Gaussian with variance $\sigma^2 \in \{10^{-5}, 10^{-4}, 10^{-3}, 10^{-2}, 10^{-1}, 1, 10\}$. As it can be seen from Figure 13.4, the average normalized error of estimating α_0 remains very low for $\sigma^2 < 0.1$, however, the performance of the algorithm decreases rapidly after $\sigma^2 = 1$.

13.7.2 Moving targets

Herein we present the simulation results for radar parameter estimation in the case of moving targets. Similar to the stationary target scenario, we assume that the noise is additive, white, and Gaussian with a variance of 0.1, and that the transmit sequence is

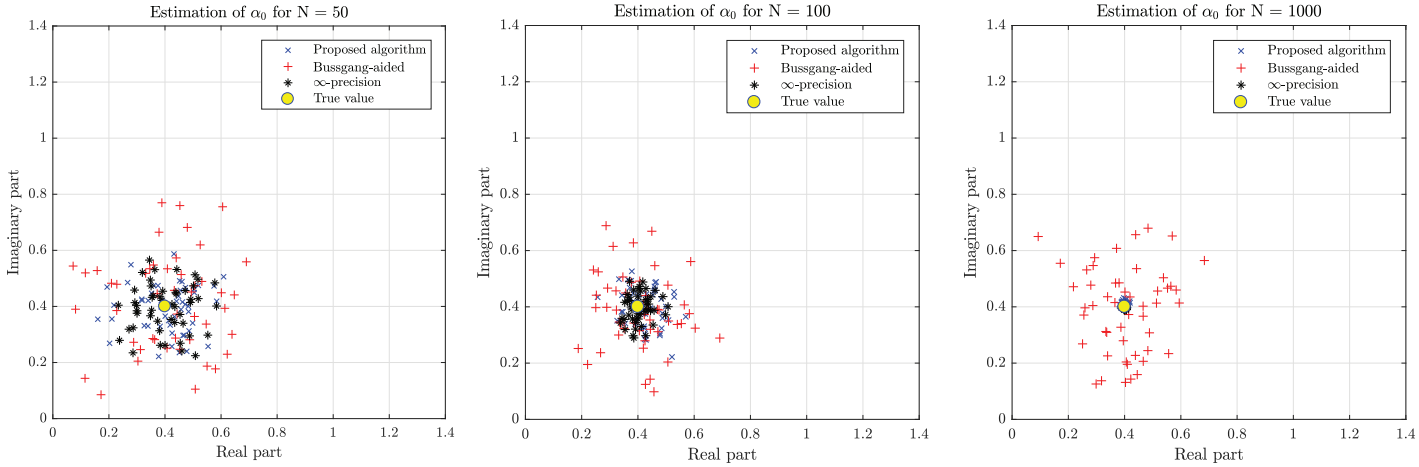

Figure 13.3 *Comparison of stationary target scattering coefficient (α_0) estimation performances for $N \in \{50, 100, 1,000\}$. The results of estimation using the proposed algorithm, the Bussgang-aided approach, and the $\infty -$ precision case are shown on complex plane along with the true value of $\alpha_0 = (0.5 + j0.5)$*

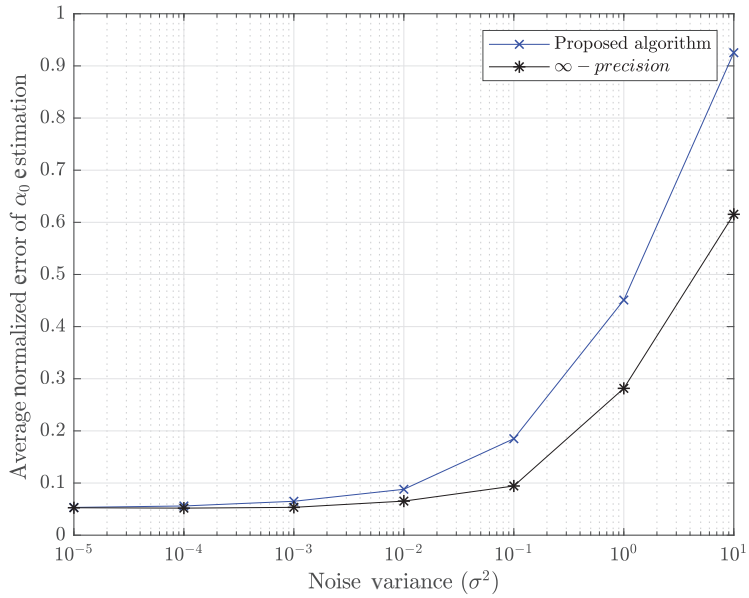

Figure 13.4 Average normalized estimation error of stationary target scattering coefficient α_0, defined by the ratio $|\alpha_0 - \hat{\alpha}_0|/|\alpha_0|$, for different noise variances $\sigma^2 \in \{10^{-5}, 10^{-4}, 10^{-3}, 10^{-2}, 10^{-1}, 1, 10\}$

generated using the method in [14] with a PAPR of 1. The number of the interfering range rings N_c and the number of azimuth sectors L are set to 2 and 10, respectively. Additionally, the normalized Doppler shifts of the adjacent range-azimuth cells are assumed to be uniformly distributed over the interval $\Omega_c = [-0.1, 0.1]$; see [66] for further details.

The estimation performance of different approaches in moving target scenarios is examined via a Monte-Carlo method with randomly generated ground truths for target parameters and presented in Figure 13.5. More precisely, the normalized estimation error of the backscattering coefficient α_0 of a moving target for the case of the proposed algorithm, as well as the Bussgang-aided approach (modified for moving targets) along with the $\infty - precision$ case are shown in Figure 13.5(a). The estimation errors for the normalized Doppler shift ν are depicted in Figure 13.5(b) for the same scenarios. Furthermore, as in the case of a stationary target, Figure 13.6 plots the radar parameter estimates for the case of a moving target through the Monte Carlo method. The upper plots in Figure 13.6 show the results of estimating the backscattering coefficient α_0, along with its true value, for $N \in \{50, 100, 1,000\}$ on the complex plane. On the other hand, the lower plots in Figure 13.6 show the estimates of the normalized Doppler shift on the polar plane. The result of estimation for different approaches is shown on circles with slightly different radii for the sake of clarity.

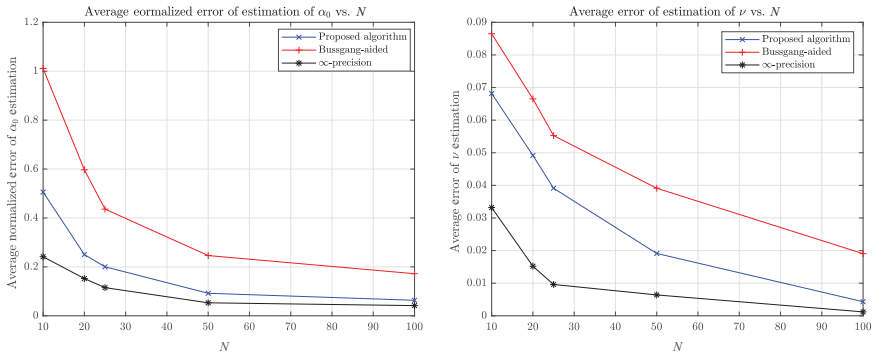

Figure 13.5 Performance comparison of moving target parameter estimation using the proposed algorithm, the Bussgang-aided approach, and the $\infty-$ precision case: (a) average normalized error of estimating the backscattering coefficient, ($|\alpha_0 - \hat{\alpha}_0|/|\alpha_0|$) and (b) average error of estimating the normalized Doppler shift ν, for different transmit sequence lengths $N \in \{10, 20, 25, 50, 100\}$

As in the case of stationary targets, it can be observed from Figure 13.5 that estimates α_0 and ν become more precise as N grows larger. In fact, as N grows large, the performance of our proposed estimator improves and gets closer to the estimate made by the ∞-precision case. Further note that in order to attain the same performance in the estimation of the parameters of a moving target, the proposed algorithm requires more samples than the stationary target case, as can be seen through Figures 13.2 and 13.5.

Finally, Figure 13.7 demonstrates the performance of the proposed algorithm in the presence of different noise power levels for the moving targets and compares it with that of ∞-precision case. For this experiment, we again use the same settings as used for the stationary case, *i.e.*, $N = 25$, and the noise is additive, white, and Gaussian with variance $\sigma^2 \in \{10^{-5}, 10^{-4}, 10^{-3}, 10^{-2}, 10^{-1}, 1, 10\}$. The average normalized error of estimating α_0 is shown in Figure 13.7(a), while the errors for estimating the normalized Doppler shift ν are depicted in Figure 13.7(b). Similar to the case of stationary targets, it can be seen from Figure 13.7 that the average error of estimating both α_0 and ν stay very low for $\sigma^2 < 0.1$, however, their performance degrades strongly after $\sigma^2 = 1$, even for ∞-precision case.

13.8 One-bit radar waveform design under uncertain statistics

In a one-bit cognitive radar system, it is often well-known that full-scale signals can indeed be recovered with high accuracy from one-bit measurements, however, at an

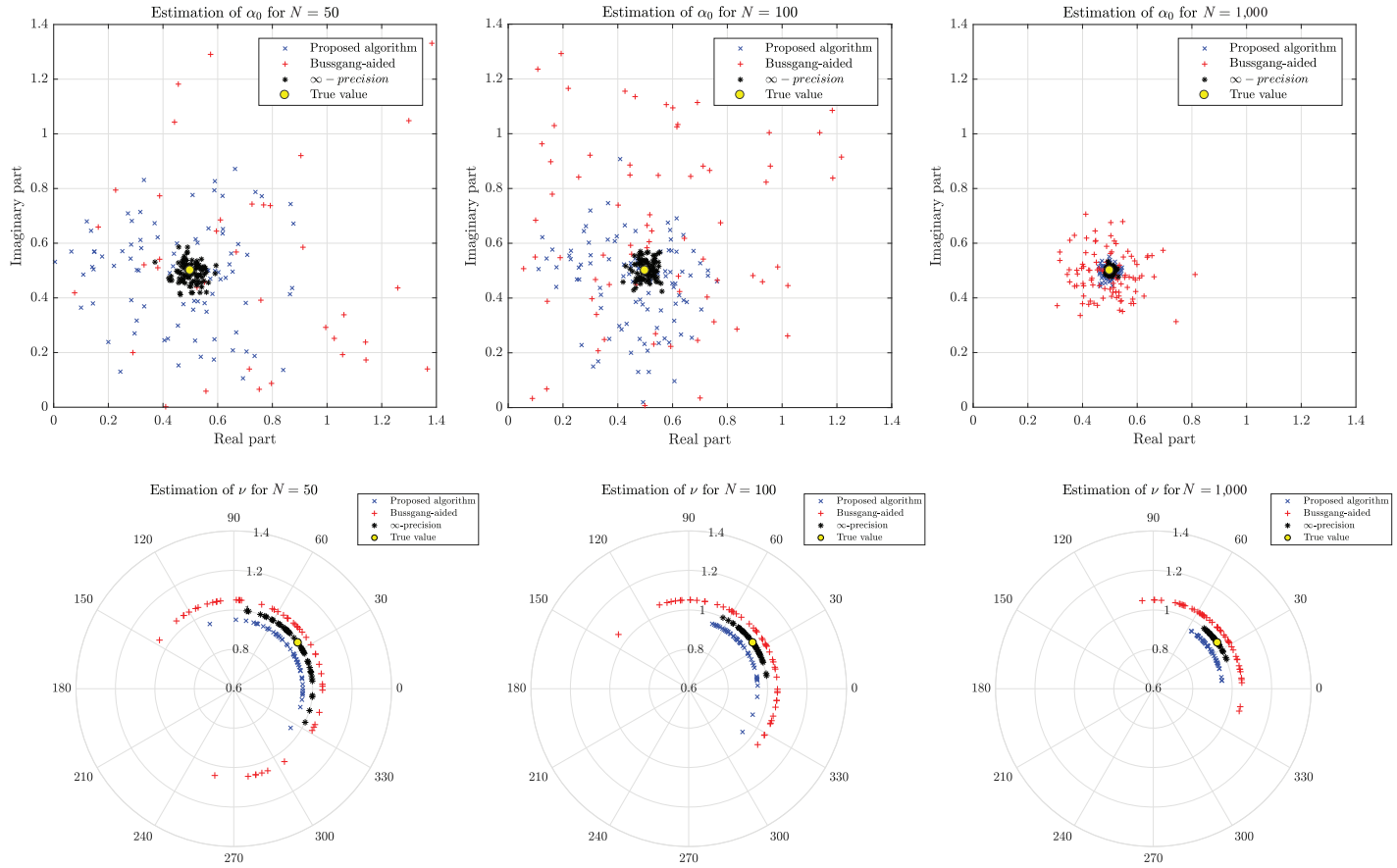

Figure 13.6 *Performance comparison of moving target parameter estimation using the proposed approach, the Bussgang-aided approach, and the $\infty -$ precision case for $N \in \{50, 100, 1,000\}$. The upper plots show the results of estimating α_0 on the complex plane, while the lower plots show the results of estimating ν on the polar plane, where different radii are used for different approaches for visual clarity.*

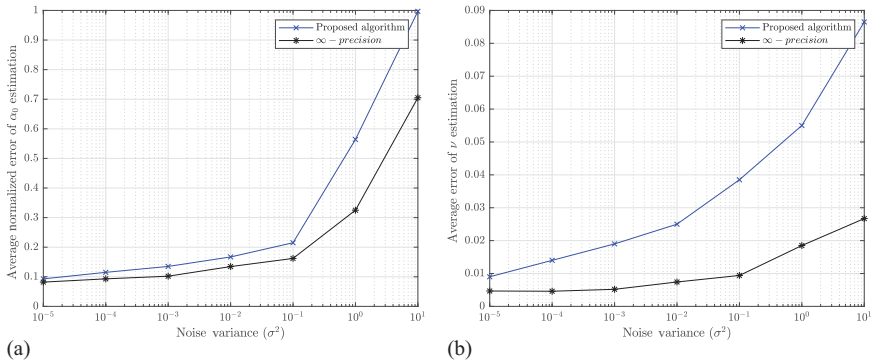

Figure 13.7 Performance comparison of moving target parameter estimation using the proposed algorithm, and the ∞-precision case: (a) average normalized error of estimating the backscattering coefficient, ($|\alpha_0 - \hat{\alpha}_0|/|\alpha_0|$); (b) average error of estimating the normalized Doppler shift ν, for different noise variances $\sigma^2 \in \{10^{-5}, 10^{-4}, 10^{-3}, 10^{-2}, 10^{-1}, 1, 10\}$

increased computational cost [67]. This increased cost mainly incurs from the fact that by using a one-bit receiver, the knowledge of interference statistics is available only in a *normalized* sense and such uncertainties prohibit one from using any traditional tools to jointly design transmit sequences, as well as the receive filter coefficients [37]. As mentioned earlier, one such traditional tool is CREW (cyclic) [14] for which the authors seek to minimize the MSE of the estimate of a target's scattering coefficient in the presence of clutter and interference and present an alternating minimization algorithm. Although this algorithm is computationally efficient, it requires full knowledge of the interference covariance matrix. In the following, we introduce a specialized variation of CREW (cyclic) to tackle the problem of jointly designing the transmit signals and the receive filter coefficients in the presence of uncertainty in interference statistics [68].

13.8.1 Problem formulation for waveform design

In the case of receivers with one-bit ADC, the quantizer is nothing but a simple sign comparator and each measurement is represented using only one bit, *i.e.*, $+1$ or -1, and the auto-correlation of the received signal is only obtainable in a *normalized* sense [54]. In particular, the matrix $\mathbf{R}$ in (13.12) is obtainable only in a normalized sense, *i.e.*, one only has access to

$$\bar{\mathbf{R}} = \boldsymbol{D}^{-\frac{1}{2}}\mathbf{R}\boldsymbol{D}^{-\frac{1}{2}}, \tag{13.43}$$

where $\boldsymbol{D} = \mathbf{R} \odot \boldsymbol{I}$. Then, the problem of interest is to design the transmit waveform $\mathbf{s}$ and the receive filter $\mathbf{w}$ given the normalized interference statistics $\bar{\mathbf{R}}$. In the following, we denote $\boldsymbol{d} = \text{diag}\left(\boldsymbol{D}^{\frac{1}{2}}\right)$.

In such a case, a meaningful approach to the aforementioned design problem is to consider minimization of the expected MSE criterion:

$$\min_{\mathbf{w},\mathbf{s}} \quad \mathbb{E}\left\{\frac{\mathbf{w}^H \boldsymbol{D}^{\frac{1}{2}} \bar{\mathbf{R}} \boldsymbol{D}^{\frac{1}{2}} \mathbf{w}}{|\mathbf{w}^H \mathbf{s}|^2}\right\}, \tag{13.44}$$

under some practical signal power constraints. Note that the expectation is taken over $\boldsymbol{D}$. The above problem is clearly non-convex. In the following, we handle the non-convexity of the optimization objective in (13.44) with respect to (w.r.t.) the probing sequence $\mathbf{s}$ and the receive filter $\mathbf{w}$ using an alternating approach and propose a specialized flavor of CREW (cyclic), named as CREW (one-bit).

13.8.2 Joint design method: CREW (one-bit)

13.8.2.1 Optimization of the radar waveform

The numerator of the MSE in (13.11) can be rearranged, for a fixed receive filter $\mathbf{w}$, as

$$\begin{aligned}\mathbf{w}^H \mathbf{R} \mathbf{w} &= \mathbf{w}^H \left(\beta \sum_{\substack{k=-N+1 \\ k\neq 0}}^{N-1} \boldsymbol{J}_k \mathbf{s}\mathbf{s}^H \boldsymbol{J}_k^H + \boldsymbol{\Gamma}\right) \mathbf{w} \\ &= \mathbf{s}^H \left(\beta \underbrace{\sum_{\substack{k=-N+1 \\ k\neq 0}}^{N-1} \boldsymbol{J}_k \mathbf{w}\mathbf{w}^H \boldsymbol{J}_k^H}_{\boldsymbol{\chi}}\right) \mathbf{s} + \mathbf{w}^H \boldsymbol{\Gamma} \mathbf{w}.\end{aligned} \tag{13.45}$$

Thus, the criterion in (13.11) can be reformulated as,

$$\frac{\text{MSE}(\hat{\alpha_0})}{\beta} = \frac{\mathbf{s}^H \boldsymbol{\chi} \mathbf{s} + \mu}{\mathbf{s}^H \mathbf{W} \mathbf{s}}, \tag{13.46}$$

where $\mu = (\mathbf{w}^H \boldsymbol{\Gamma} \mathbf{w})/\beta$ and $\mathbf{W} = \mathbf{w}\mathbf{w}^H$. It is interesting to note that μ is unknown; however, independent of $\mathbf{s}$, and thus merely a constant scalar w.r.t. $\mathbf{s}$. To deal with the optimization problem of (13.46), we follow the identical framework as [14] that exploits the idea of fractional programming [69].

Let $a(\mathbf{s}) = \mathbf{s}^H \boldsymbol{\chi} \mathbf{s} + \mu$, and $b(\mathbf{s}) = \mathbf{s}^H \mathbf{W} \mathbf{s} > 0$ (MSE needs to be finite). Further, let $f(\mathbf{s}) = a(\mathbf{s})/b(\mathbf{s})$ and $\mathbf{s}_*$ denote the current value of $\mathbf{s}$. We define $g(\mathbf{s}) \triangleq a(\mathbf{s}) - f(\mathbf{s}_*) b(\mathbf{s})$, and $\mathbf{s}_\dagger \triangleq \arg\min_{\mathbf{s}} g(\mathbf{s})$. It can be easily verified that $g(\mathbf{s}_\dagger) \leq g(\mathbf{s}_*) = 0$. As a result, we have that $g(\mathbf{s}_\dagger) = a(\mathbf{s}_\dagger) - f(\mathbf{s}_*) b(\mathbf{s}_\dagger) \leq 0$ which indicates to $f(\mathbf{s}_\dagger) \leq f(\mathbf{s}_*)$ as $b(\mathbf{s}_\dagger) > 0$. Therefore, $\mathbf{s}_\dagger$ can be considered as a new vector $\mathbf{s}$ that monotonically

decreases $f(\mathbf{s})$. Note that $\mathbf{s}_\dagger$ does not necessarily have to be a minimizer of $g(\mathbf{s})$; instead, it is enough if $g(\mathbf{s}_\dagger) \leq g(\mathbf{s}_*)$.

Under the assumption that $\|\mathbf{s}\|_2^2 = N$, for a fixed $\mathbf{w}$ and any arbitrary $\mathbf{s}_*$ of the minimizer $\mathbf{s}$ of (13.46), we have:

$$g(\mathbf{s}) = \mathbf{s}^H(\boldsymbol{\chi} - f(\mathbf{s}_*)\mathbf{W})\mathbf{s} + \mu = \mathbf{s}^H \boldsymbol{T}\mathbf{s} + \mu, \tag{13.47}$$

where $\boldsymbol{T} \triangleq \boldsymbol{\chi} - f(\mathbf{s}_*)\mathbf{W}$. Then the problem of (13.46) w.r.t. unimodular $\mathbf{s}$ can be recast as the following unimodular quadratic program (UQP) [70]:

$$\max_{\mathbf{s}} \ \mathbf{s}^H \tilde{\boldsymbol{T}}\mathbf{s} \qquad \text{s.t. } |s_k| = 1, \qquad 1 \leq k \leq N, \tag{13.48}$$

where $\tilde{\boldsymbol{T}} \triangleq \lambda \boldsymbol{I} - \boldsymbol{T}$ is a positive definite matrix and λ is a real scalar greater than the maximum eigenvalue of $\boldsymbol{T}$. Note that (13.48) is NP-hard in general, and a sub-optimal solution can be sought by semi-definite relaxation (SDR). To tackle this problem efficiently, in [70] a set of *power method-like* iterations was suggested that can be used to monotonically increase the criterion in (13.48); namely, the vector $\mathbf{s}$ is updated in each iteration n using the nearest-vector problem:

$$\begin{aligned} \min_{\mathbf{s}^{(n+1)}} \quad & \left\| \mathbf{s}^{(n+1)} - \tilde{\boldsymbol{T}}\mathbf{s}^{(n)} \right\|_2 \\ \text{s.t.} \quad & \left| s_k^{(n+1)} \right| = 1, \qquad 1 \leq k \leq N. \end{aligned} \tag{13.49}$$

Fortunately, the solution to (13.49) is simply given analytically by $\mathbf{s}^{(n+1)} = e^{j \arg(\tilde{\boldsymbol{T}}\mathbf{s}^{(n)})}$. A proof of monotonically increasing behavior of the UQP objective in (13.48) can be found in [14].

13.8.2.2 Optimization of the receive filter

For a fixed $\mathbf{s}$, the objective of (13.44) can be further simplified as,

$$\begin{aligned} \mathbb{E}\left\{ \frac{\mathbf{w}^H \boldsymbol{D}^{\frac{1}{2}} \bar{\mathbf{R}} \boldsymbol{D}^{\frac{1}{2}} \mathbf{w}}{|\mathbf{w}^H \mathbf{s}|^2} \right\} &= \frac{\mathbb{E}\left\{ \mathrm{tr}\left(\mathbf{w}\mathbf{w}^H \boldsymbol{D}^{\frac{1}{2}} \bar{\mathbf{R}} \boldsymbol{D}^{\frac{1}{2}} \right) \right\}}{|\mathbf{w}^H \mathbf{s}|^2} \\ &= \frac{\mathbb{E}\left\{ \boldsymbol{d}^H \left(\mathbf{w}\mathbf{w}^H \odot \bar{\mathbf{R}}^H \right) \boldsymbol{d} \right\}}{|\mathbf{w}^H \mathbf{s}|^2} \\ &= \frac{\mathrm{tr}\left(\left(\mathbf{w}\mathbf{w}^H \odot \bar{\mathbf{R}}^H \right) \mathbb{E}\left\{ \boldsymbol{d}\boldsymbol{d}^H \right\} \right)}{|\mathbf{w}^H \mathbf{s}|^2}. \end{aligned} \tag{13.50}$$

It is evident that the knowledge of $\boldsymbol{d}$ indirectly demands more information on β and $\boldsymbol{\Gamma}$. However, assuming the statistics of the noise is unchanging, one can estimate $\boldsymbol{\Gamma}$ in a normalized sense by just listening to the environment while not transmitting any waveform. As a result, from the one-bit receiver, the normalized interference covariance matrix $\bar{\boldsymbol{\Gamma}}$ can be obtained in a similar fashion as, $\bar{\boldsymbol{\Gamma}} \triangleq \boldsymbol{A}^{-\frac{1}{2}} \boldsymbol{\Gamma} \boldsymbol{A}^{-\frac{1}{2}}$, where $\boldsymbol{A} = \boldsymbol{\Gamma} \odot \boldsymbol{I}$. Thus, the interference covariance matrix $\mathbf{R}$ in (13.12) can be reformulated as,

$$\mathbf{R} = \boldsymbol{D}^{\frac{1}{2}} \bar{\mathbf{R}} \boldsymbol{D}^{\frac{1}{2}} = \beta \mathbf{S} + \boldsymbol{A}^{\frac{1}{2}} \bar{\boldsymbol{\Gamma}} \boldsymbol{A}^{\frac{1}{2}}, \tag{13.51}$$

where $\mathbf{S} = \sum_{k \neq 0} \boldsymbol{J}_k \mathbf{s}\mathbf{s}^H \boldsymbol{J}_k^H$ is constant for a known $\mathbf{s}$. Hence, a judicious approach is to solve the following problem in order to optimize $\boldsymbol{d}, \boldsymbol{a}$, and β in a joint manner:

$$\{\hat{\boldsymbol{d}}, \hat{\boldsymbol{a}}, \hat{\beta}\} = \arg\min_{\boldsymbol{d},\boldsymbol{a},\beta} \quad \left\| \text{Diag}\,(\boldsymbol{d})^{\frac{1}{2}} \ \bar{\mathbf{R}} \ \text{Diag}\,(\boldsymbol{d})^{\frac{1}{2}} - \beta \mathbf{S} + \text{Diag}\,(\boldsymbol{a})^{\frac{1}{2}} \ \bar{\boldsymbol{\Gamma}} \ \text{Diag}\,(\boldsymbol{a})^{\frac{1}{2}} \right\|_F^2,$$
$$\text{s.t.} \quad \boldsymbol{d} > 0, \boldsymbol{a} > 0, \beta > 0. \tag{13.52}$$

The above minimization problem is non-convex, and, hence, in order to efficiently solve it, we resort to an alternating approach; *i.e.*, solving for each variable while keeping the other two variables as constant. By doing so, w.r.t. each variable, the problem becomes convex and can be solved using a number of available numerical solvers, such as the "fmincon" function in MATLAB® that implements the Broyden–Fletcher–Goldfarb–Shanno (BFGS) algorithm. Note that by solving (13.52), one can obtain β and $\boldsymbol{d}$ in an average sense, which in other words justifies the usage of expectation in the formulation of (13.50).

With this information in mind, let $\sum_{k=1}^{N} \nu_k \boldsymbol{u}_k \boldsymbol{u}_k^H$ represent the eigenvalue decomposition (EVD) of $\mathbb{E}\left\{\boldsymbol{d}\boldsymbol{d}^H\right\}$, where $\{\nu_k\}$ and $\{\boldsymbol{u}_k\}$ represent the eigenvalues and the eigenvectors, respectively. As a result, the numerator of (13.50) can be further simplified as,

$$\begin{aligned}
\text{tr}\left(\left(\mathbf{w}\mathbf{w}^H \odot \bar{\mathbf{R}}^H\right) \sum_{k=1}^{N} \nu_k \boldsymbol{u}_k \boldsymbol{u}_k^H\right) &= \sum_{k=1}^{N} \nu_k \boldsymbol{u}_k^H \left(\mathbf{w}\mathbf{w}^H \odot \bar{\mathbf{R}}^H\right) \boldsymbol{u}_k \\
&= \left(\mathbf{w}\mathbf{w}^H\right) \sum_{k=1}^{N} \nu_k \ \text{Diag}\,(\boldsymbol{u}_k) \ \bar{\mathbf{R}} \ \text{Diag}\left(\boldsymbol{u}_k^H\right) \\
&= \mathbf{w}^H \boldsymbol{Q} \mathbf{w},
\end{aligned} \tag{13.53}$$

where

$$\boldsymbol{Q} = \sum_{k=1}^{N} \nu_k \ \text{Diag}\,(\boldsymbol{u}_k) \ \bar{\mathbf{R}} \ \text{Diag}\left(\boldsymbol{u}_k^H\right). \tag{13.54}$$

It is interesting to note that $\boldsymbol{Q}$ can be viewed as the expected value of $\mathbf{R}$. By using $\boldsymbol{D}^{\frac{1}{2}} = \text{Diag}\,(\boldsymbol{d})$, the following can be deduced:

$$\mathbb{E}\{\mathbf{R}\} = \mathbb{E}\left\{\boldsymbol{D}^{\frac{1}{2}} \bar{\mathbf{R}} \boldsymbol{D}^{\frac{1}{2}}\right\} = \mathbb{E}\left\{\boldsymbol{d}\boldsymbol{d}^H\right\} \odot \bar{\mathbf{R}}. \tag{13.55}$$

Assuming $\mathbb{E}\left\{\boldsymbol{d}\boldsymbol{d}^H\right\} = \boldsymbol{\eta}\boldsymbol{\eta}^H + \boldsymbol{\Sigma}$, (13.55) can be reformulated as

$$\begin{aligned}
\mathbb{E}\{\mathbf{R}\} &= (\boldsymbol{\eta}\boldsymbol{\eta}^H + \boldsymbol{\Sigma}) \odot \bar{\mathbf{R}} \\
&= \sum_{k=1}^{N} \nu_k \boldsymbol{u}_k \boldsymbol{u}_k^H \odot \bar{\mathbf{R}} \\
&= \sum_{k=1}^{N} \nu_k \ \text{Diag}\,(\boldsymbol{u}_k) \ \bar{\mathbf{R}} \ \text{Diag}\left(\boldsymbol{u}_k^H\right),
\end{aligned} \tag{13.56}$$

which proves the claim.

Algorithm 3: CREW (ONE-BIT)

Ensure: $\mathbf{s}^{(0)} \leftarrow$ unimodular (or low PAPR) vector in $\mathbb{C}^N$, $\mathbf{w}^{(0)} \leftarrow$ random vector in $\mathbb{C}^N$, the outer loop index $t \leftarrow 1$.

1: **repeat**
2: **For fixed w**,
i) Compute $\boldsymbol{\chi}, \mathbf{W}$ using (13.45), and thus, in turn find $\tilde{\boldsymbol{T}}$.
ii) Solve the power method like iterations discussed in (13.49), and calculate $\mathbf{s}^{(t)}$ in each iteration until convergence.
3: Measure $\bar{\boldsymbol{\Gamma}}$ at the output of the one-bit receiver and compute $\bar{\mathbf{R}}$ using $\mathbf{s}^{(t)}$.
4: **For fixed s**,
i) Solve (13.52) to obtain $\boldsymbol{d}$ and β in average sense.
ii) Compute the EVD of $\mathbb{E}\left\{\boldsymbol{d}\boldsymbol{d}^H\right\}$, and form $\boldsymbol{Q}$.
iii) Update $\mathbf{w}^{(t)}$ as $\boldsymbol{Q}^{-1}\mathbf{s}^{(t)}$.
5: **until** convergence, *e.g.*, $\left|\mathrm{MSE}^{(t+1)} - \mathrm{MSE}^{(t)}\right| < \varepsilon$ for some given $\varepsilon > 0$.

In light of the above, the receive filter optimization problem translates to:

$$\min_{\mathbf{w}} \ \frac{\mathbf{w}^H \boldsymbol{Q} \mathbf{w}}{|\mathbf{w}^H \mathbf{s}|^2}. \tag{13.57}$$

Hence, for a given $\mathbf{s}$, the optimization problem in (13.57) w.r.t. $\mathbf{w}$ results in the closed-form solution, $\mathbf{w} = \boldsymbol{Q}^{-1}\mathbf{s}$, within a multiplicative constant. Finally, the algorithm CREW (one-bit) is summarized in Algorithm 3 in a concise manner.

13.9 Waveform design examples

In this section, we evaluate the performance of CREW (one-bit) and compare it with three state-of-the-art methods, namely CAN-MMF, CREW (fre), and CREW (cyclic). The CAN-MMF method employs the CAN algorithm in [15] to simply design a transmit waveform with good correlation properties and independent of the receive filter. Note that no prior knowledge of interference is used in the waveform design of CAN-MMF.

We adopt the same simulation setups as in [14]. Especially, for the interference covariance matrix, we consider the following:

$$\boldsymbol{\Gamma} = \sigma_J^2 \boldsymbol{\Gamma}_J + \sigma^2 \boldsymbol{I},$$

where $\sigma_J^2 = 100$, and $\sigma^2 = 0.1$ are the jamming and noise powers, respectively. Furthermore, the jamming covariance matrix $\boldsymbol{\Gamma}_J$ is given by $[\boldsymbol{\Gamma}_J]_{k,l} = \gamma_{k-l}$ where $[\gamma_0, \gamma_1, \cdots, \gamma_{N-1}, \gamma_{-(N-1)}, \cdots, \gamma_{-1}]^T$ can be obtained by an inverse FFT (IFFT) of the jamming power spectrum $\{\eta_p\}$ at frequencies $(p-1)/(2N-1)$, $p = 1, \cdots, 2N-1$. For CREW(fre) and CREW(cyclic), we fix the average clutter power to $\beta = 1$. Finally,

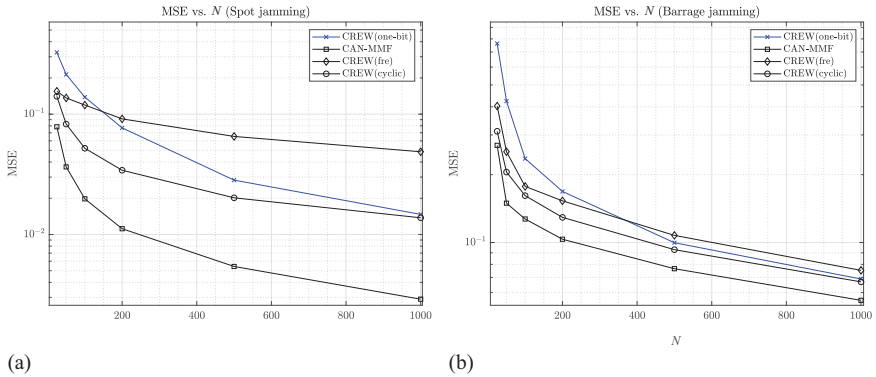

Figure 13.8 MSE values obtained by the different design algorithms for (a) spot jamming with normalized frequency $f_0 = 0.2$, and (b) barrage jamming in the normalized frequency interval $[f_1, f_2] = [0.2, 0.3]$ for the unimodularity constraint on the transmit sequence

we use the Golomb sequence in order to initialize the transmit waveform $\mathbf{s}$ for all algorithms.

We consider two modes of jamming: spot and barrage. Spot jamming is concentrated power directed toward one channel or frequency. In our example, we use a spot jamming located at a normalized frequency $f_0 = 0.2$. On the other hand, barrage jamming is power spread over several frequencies or channels at the same time. We consider a barrage jamming located in the normalized frequency bands $[f_1, f_2] = [0.2, 0.3]$.

Figure 13.8(a) and (b) depict the MSE values for spot and barrage jamming, respectively, corresponding to CAN-MMF, CREW(fre), and CREW(cyclic), under the unimodularity constraint, for various sequence lengths. It is evident from the figures that when the sequence length N is small, the MSE is higher for CREW (one-bit) compared to other algorithms. However, as N increases, CREW (one-bit) shows similar performance as CREW (cyclic), and eventually, they coincide with one another for higher values of N. Consequently, it is implied that higher signal length introduces more degrees of freedom in designing transmit waveform and thus, compensates for the uncertainties in interference statistics. It is further important to observe that the knowledge of the one-bit measurements impacts the design of the receive filter, and alternatively, the design of the receive filter coefficients impacts the design of transmit waveform, which justifies the role of a cognitive radar.

13.10 Concluding remarks

High-resolution sampling with conventional analog-to-digital converters (ADCs) can be very costly and energy-consuming for many modern applications. This is further

accentuated as recent applications, including those in sensing and radar signal processing, show a growing appetite in even larger than usual sampling rates—thus making the mainstream ADCs a rather unsuitable choice. To overcome these shortcomings, it was shown that in lieu of using the conventional ADCs in radar parameters estimation, one can use inexpensive comparators with time-varying thresholds and solve an optimization problem to recover the target parameters with satisfactory performance. This is very beneficial at high frequencies as it is both practical and economical, while it can also pave the way for future applications to sample at much higher rates. Simulation results were presented that verify the efficiency of one-bit target parameter estimation for both stationary and moving targets, especially as the length of the transmit sequence N grows large. Finally, radar waveform and receive filter design were studied under uncertain statistics that are common due to low-resolution sampling.

References

[1] Stepanenko VD. *Radar in Meteorology*. Wright-Patterson AFB, OH: Foreign Technology Div; 1975.

[2] Browning K. Uses of radar in meteorology. *Contemporary Physics*. 1986;27(6): 499–517. Available from: https://doi.org/10.1080/00107518608211028.

[3] Bussolari S, Bernays J. Mode S data link applications for general aviation. In: *Proceedings of 14th Digital Avionics Systems Conference*; 1995. p. 199–206.

[4] Nolan M. Fundamentals of air traffic control. In: *Cengage Learning*. Boston, MA: Cengage; 2010.

[5] Ihn JB and Chang FK. Pitch-catch active sensing methods in structural health monitoring for aircraft structures. *Structural Health Monitoring*. 2008;7(1): 5–19.

[6] Lynch JP, Sundararajan A, Law KH, *et al*. Design of a wireless active sensing unit for structural health monitoring. In: *Health Monitoring and Smart Nondestructive Evaluation of Structural and Biological Systems III*, vol. 5394. International Society for Optics and Photonics; 2004. p. 157–169.

[7] Soumekh M. *Synthetic Aperture Radar Signal Processing*, vol. 7. New York: Wiley; 1999.

[8] Curlander JC and McDonough RN. *Synthetic Aperture Radar*, vol. 396. New York, NY: John Wiley & Sons; 1991.

[9] Heidemann J, Stojanovic M, and Zorzi M. Underwater sensor networks: applications, advances and challenges. *Philosophical Transactions of the Royal Society A*. 2012;370(1958):158–175.

[10] Farr N, Bowen A, Ware J, *et al*. An integrated, underwater optical/acoustic communications system. In: *OCEANS*. IEEE; 2010. p. 1–6.

[11] He H, Li J, and Stoica P. *Waveform Design for Active Sensing Systems: A Computational Approach*. Cambridge: Cambridge University Press; 2012.

[12] Haykin S. Cognitive radar: a way of the future. *IEEE Signal Processing Magazine*. 2006;23(1):30–40.

[13] Levanon N and Mozeson E. *Radar Signals*. New York, NY: John Wiley & Sons; 2004.
[14] Soltanalian M, Tang B, Li J, *et al*. Joint design of the receive filter and transmit sequence for active sensing. *IEEE Signal Processing Letters*. 2013;20(5): 423–426.
[15] Stoica P, He H, and Li J. New algorithms for designing unimodular sequences with good correlation properties. *IEEE Transactions on Signal Processing*. 2009;57(4):1415–1425.
[16] Soltanalian M and Stoica P. Computational design of sequences with good correlation properties. *IEEE Transactions on Signal Processing*. 2012;60(5):2180–2193.
[17] Bose A and Soltanalian M. Constructing binary sequences with good correlation properties: an efficient analytical-computational interplay. *IEEE Transactions on Signal Processing*. 2018;66(11):2998–3007.
[18] Woodward PM. *Probability and Information Theory, with Applications to Radar: International Series of Monographs on Electronics and Instrumentation*, vol. 3. Amsterdam: Elsevier; 2014.
[19] Sussman S. Least-square synthesis of radar ambiguity functions. *IRE Transactions on Information Theory*. 1962;8(3):246–254.
[20] Wolf JD, Lee GM, and Suyo CE. Radar waveform synthesis by mean square optimization techniques. *IEEE Transactions on Aerospace and Electronic Systems*. 1969;AES-5(4):611–619.
[21] Wu L, Babu P, and Palomar DP. Cognitive radar-based sequence design via SINR maximization. *IEEE Transactions on Signal Processing*. 2017;65(3):779–793.
[22] Stoica P, Li J, and Xue M. Transmit codes and receive filters for radar. *IEEE Signal Processing Magazine*. 2008;25(6):94–109.
[23] Spafford L. Optimum radar signal processing in clutter. *IEEE Transactions on Information Theory*. 1968;14(5):734–743. Available from: https://doi.org/10.1109/TIT.1968.1054205.
[24] Stoica P, He H, and Li J. Optimization of the receive filter and transmit sequence for active sensing. *IEEE Transactions on Signal Processing*. 2012;60(4): 1730–1740.
[25] Rummler WD. A technique for improving the clutter performance of coherent pulse train signals. *IEEE Transactions on Aerospace and Electronic Systems*. 1967;AES-3:898–906.
[26] Pillai SU, Youla DC, Oh HS, *et al*. Optimum transmit-receiver design in the presence of signal-dependent interference and channel noise. In: *Conference Record of the 33rd Asilomar Conference on Signals, Systems, and Computers, 1999*, vol. 2. Piscataway, NJ: IEEE; 1999. p. 870–875.
[27] DeLong D and Hofstetter E. On the design of optimum radar waveforms for clutter rejection. *IEEE Transactions on Information Theory*. 1967;13(3): 454–463.
[28] Bell MR. Information theory and radar waveform design. *IEEE Transactions on Information Theory*. 1993;39(5):1578–1597.

[29] Kay S. Optimal signal design for detection of Gaussian point targets in stationary clutter/reverberation. *IEEE Journal of Selected Topics in Signal Processing*. 2007;1(1):31–41.

[30] Naghsh MM, Soltanalian M, Stoica P, *et al*. A Doppler robust design of transmit sequence and receive filter in the presence of signal-dependent interference. *IEEE Transactions on Signal Processing*. 2014;62(4):772–785.

[31] Gianelli C, Xu L, Li J, *et al*. One-bit compressive sampling with time-varying thresholds for sparse parameter estimation. In: *Sensor Array and Multichannel Signal Processing Workshop (SAM), 2016 IEEE*. Piscataway, NJ: IEEE; 2016. p. 1–5.

[32] Sun H, Nallanathan A, Wang CX, *et al*. Wideband spectrum sensing for cognitive radio networks: a survey. *IEEE Wireless Communications*. 2013;20(2):74–81.

[33] Lunden J, Koivunen V, and Poor HV. Spectrum exploration and exploitation for cognitive radio: Recent advances. *IEEE Signal Processing Magazine*. 2015;32(3):123–140.

[34] Burke BF and Graham-Smith F. *An Introduction to Radio Astronomy*. Cambridge: Cambridge University Press; 2009.

[35] Strohm KM, Bloecher HL, Schneider R, *et al*. Development of future short range radar technology. In: *Radar Conference, 2005. EURAD 2005. European*. Piscataway, NJ: IEEE; 2005. p. 165–168.

[36] Hasch J, Topak E, Schnabel R, *et al*. Millimeter-wave technology for automotive radar sensors in the 77 GHz frequency band. *IEEE Transactions on Microwave Theory and Techniques*. 2012;60(3):845–860.

[37] Khobahi S and Soltanalian M. Signal recovery from 1-bit quantized noisy samples via adaptive thresholding. In: *2018 52nd Asilomar Conference on Signals, Systems, and Computers*; 2018. p. 1757–1761.

[38] Ribeiro A and Giannakis GB. Bandwidth-constrained distributed estimation for wireless sensor networks—Part I: Gaussian case. *IEEE Transactions on Signal Processing*. 2006;54(3):1131–1143.

[39] Ribeiro A and Giannakis GB. Bandwidth-constrained distributed estimation for wireless sensor networks—Part II: unknown probability density function. *IEEE Transactions on Signal Processing*. 2006;54(7):2784–2796.

[40] Host-Madsen A and Handel P. Effects of sampling and quantization on single-tone frequency estimation. *IEEE Transactions on Signal Processing*. 2000;48(3):650–662.

[41] Bar-Shalom O and Weiss AJ. DOA estimation using one-bit quantized measurements. *IEEE Transactions on Aerospace and Electronic Systems*. 2002;38(3):868–884.

[42] Dabeer O and Karnik A. Signal parameter estimation using 1-bit dithered quantization. *IEEE Transactions on Information Theory*. 2006;52(12): 5389–5405.

[43] Dabeer O and Masry E. Multivariate signal parameter estimation under dependent noise from 1-bit dithered quantized data. *IEEE Transactions on Information Theory*. 2008;54(4):1637–1654.

[44] Khobahi S, Naimipour N, Soltanalian M, *et al*. Deep signal recovery with one-bit quantization. In: *2019 IEEE International Conference on Acoustics, Speech and Signal Processing (ICASSP)*; 2019. p. 2987–2991.
[45] Hu H, Soltanalian M, Stoica P, *et al*. Locating the few: sparsity-aware waveform design for active radar. *IEEE Transactions on Signal Processing*. 2017;65(3):651–662.
[46] Boufounos P and Baraniuk R. 1-Bit compressive sensing. In: *42nd Annual Conference on Information Sciences and Systems*; 2008. p. 16–21.
[47] Knudson K, Saab R, and Ward R. One-bit compressive sensing with norm estimation. *IEEE Transactions on Information Theory*. 2016;62(5):2748–2758.
[48] Zymnis A, Boyd S, and Candes E. Compressed sensing with quantized measurements. *IEEE Signal Processing Letters*. 2010;17(2):149–152.
[49] Plan Y and Vershynin R. Robust 1-bit compressed sensing and sparse logistic regression: a convex programming approach. *IEEE Transactions on Information Theory*. 2013;59(1):482–494.
[50] Dong X and Zhang Y. A MAP approach for 1-bit compressive sensing in synthetic aperture radar imaging. *IEEE Geoscience and Remote Sensing Letters*. 2015;12(6):1237–1241.
[51] Masry E. *The Reconstruction of Analog Signals from the Sign of Their Noisy Samples*. California University of San Diego, La Jolla, Department of Electrical Engineering and Computer Sciences; 1980.
[52] Cvetkovic Z and Daubechies I. Single-bit oversampled A/D conversion with exponential accuracy in the bit-rate. In: *Data Compression Conference, 2000. Proceedings. DCC 2000*. Piscataway, NJ: IEEE; 2000. p. 343–352.
[53] Cheng Z, Liao B, He Z, *et al*. Transmit signal design for large-scale MIMO system with 1-bit DACs. *IEEE Transactions on Wireless Communications*. 2019;18(9):4466–4478.
[54] Ameri A, Bose A, Li J, *et al*. One-bit radar processing with time-varying sampling thresholds. *IEEE Transactions on Signal Processing*. 2019;67(20): 5297–5308.
[55] Blunt S and Gerlach K. Adaptive pulse compression via MMSE estimation. *IEEE Transactions on Aerospace and Electronic Systems*. 2006;42(2):572–584.
[56] Bussgang JJ. *Cross-correlation Functions of Amplitude-Distorted Gaussian Signals*. Cambridge, MA: MIT Res. Lab.; 1952.
[57] Van Vleck JH and Middleton D. The spectrum of clipped noise. *Proceedings of the IEEE*. 1966;54(1):2–19.
[58] Liu CL and Vaidyanathan PP. One-bit sparse array DOA estimation. In: *2017 IEEE International Conference on Acoustics, Speech and Signal Processing (ICASSP)*. Piscataway, NJ: IEEE; 2017. p. 3126–3130.
[59] Bro R and De Jong S. A fast non-negativity-constrained least squares algorithm. *Journal of Chemometrics*. 1997;11(5):393–401.
[60] Aubry A, Maio AD, Piezzo M, *et al*. Cognitive design of the receive filter and transmitted phase code in reverberating environment. *IET Radar, Sonar Navigation*. 2012;6(9):822–833.

[61] Gini F, De Maio A, and Patton L. *Waveform Design and Diversity for Advanced Radar Systems*. London: Institution of Engineering and Technology; 2012.
[62] Aubry A, Maio AD, Farina A, *et al*. Knowledge-aided (potentially cognitive) transmit signal and receive filter design in signal-dependent clutter. *IEEE Transactions on Aerospace and Electronic Systems*. 2013;49(1):93–117.
[63] Wang CJ, Wen BY, Ma ZG, *et al*. Measurement of river surface currents with UHF FMCW radar systems. *Journal of Electromagnetic Waves and Applications*. 2007;21(3):375–386. Available from: https://doi.org/10.1163/156939307779367350.
[64] Kondo M, Kawai K, Hirano H, *et al*. Ocean wave observation by CW mm-wave radar with narrow beam. In: *Proceedings of the 2001 IEEE Radar Conference*; 2001. p. 398–403.
[65] Stoica P and Moses RL. *Spectral Analysis of Signals*. Englewood Cliffs, NJ: Pearson/Prentice Hall; 2005.
[66] Skolnik MI. *Radar Handbook*. New York, NY: McGraw-Hill; 1970.
[67] Laska JN, Wen Z, Yin W, *et al*. Trust, but verify: fast and accurate signal recovery from 1-bit compressive measurements. *IEEE Transactions on Signal Processing*. 2011;59(11):5289–5301.
[68] Bose A, Ameri A, and Soltanalian M. Waveform design for one-bit radar systems under uncertain interference statistics. In: *2019 53rd Asilomar Conference on Signals, Systems, and Computers*; 2019. p. 1167–1171.
[69] Dinkelbach W. On nonlinear fractional programming. *Management Science*. 1967;13(7):492–498. Available from: http://www.jstor.org/stable/2627691.
[70] Soltanalian M and Stoica P. Designing unimodular codes via quadratic optimization. *IEEE Transactions on Signal Processing*. 2014;62(5):1221–1234.

Chapter 13

One-bit cognitive radar

Author Queries

AQ1: Please provide department details and city name to be consistent with other chapters.